Article

Current Biology

Dual Role of an *mps-2/KCNE*-Dependent Pathway in Long-Term Memory and Age-Dependent Memory Decline

Graphical Abstract

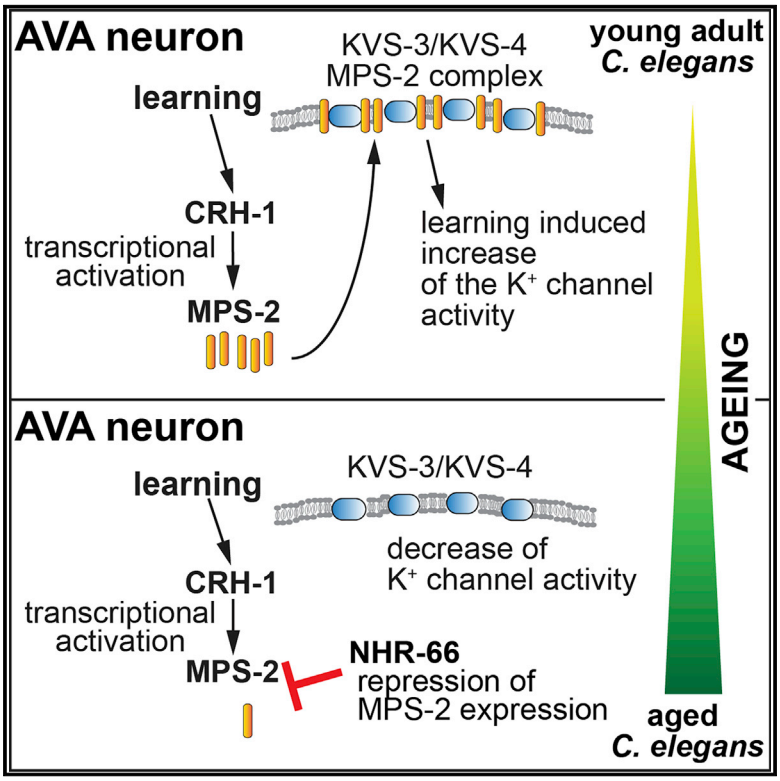

Authors

Bank G. Fenyves, Andreas Arnold, Vaibhav G. Gharat, ..., Dominique de Quervain, Andreas Papassotiropoulos, Attila Stetak

Correspondence

a.stetak@unibas.ch

In Brief

Fenyves et al. report a conserved MPS-2/KVS-3/KVS-4 pathway essential for long-term associative memory in *C. elegans*. Furthermore, MPS-2 controls age-dependent memory decline being the target of a controlled repression mechanism mediated by NHR-66. These results provide a link between a conserved memory pathway and age-dependent memory decline.

Highlights

- MPS-2/KCNE controls long-term associative memory
- MPS-2 is in complex and acts through KVS-3 and KVS-4 voltage-gated K^+ channels
- Age-dependent memory decline is linked to MPS-2 expression levels
- NHR-66 actively represses MPS-2 expression, controlling age-dependent memory decline

Fenyves et al., 2021, Current Biology *31*, 527–539
February 8, 2021
https://doi.org/10.1016/j.cub.2020.10.069

CellPress

Current Biology

CellPress
OPEN ACCESS

Article

Dual Role of an *mps-2/KCNE*-Dependent Pathway in Long-Term Memory and Age-Dependent Memory Decline

Bank G. Fenyves,[1,2,7,8] Andreas Arnold,[1,2,8] Vaibhav G. Gharat,[1,2,8] Carmen Haab,[2] Kiril Tishinov,[3] Fabian Peter,[1,2] Dominique de Quervain,[1,5,6] Andreas Papassotiropoulos,[1,2,4,6] and Attila Stetak[1,2,6,9,*]

[1]Transfaculty Research Platform Molecular and Cognitive Neurosciences, University of Basel, Birmannsgasse 8, 4055 Basel, Switzerland
[2]Division of Molecular Neuroscience, Department of Psychology, University of Basel, Birmannsgasse 8, 4055 Basel, Switzerland
[3]Biozentrum, University of Basel, Klingelbergstrasse 50/70, 4056 Basel, Switzerland
[4]Biozentrum, Life Sciences Training Facility, University of Basel, Klingelbergstrasse 50/70, 4056 Basel, Switzerland
[5]Division of Cognitive Neuroscience, Department of Psychology, University of Basel, Birmannsgasse 8, 4055 Basel, Switzerland
[6]University Psychiatric Clinics, University of Basel, Wilhelm Klein-Strasse 27, 4055 Basel, Switzerland
[7]Department of Molecular Biology, Semmelweis University, Tűzoltó u. 37-47, 1094 Budapest, Hungary
[8]These authors contributed equally
[9]Lead Contact
*Correspondence: a.stetak@unibas.ch
https://doi.org/10.1016/j.cub.2020.10.069

SUMMARY

Activity-dependent persistent changes in neuronal intrinsic excitability and synaptic strength are underlying learning and memory. Voltage-gated potassium (K_v) channels are potential regulators of memory and may be linked to age-dependent neuronal disfunction. MinK-related peptides (MiRPs) are conserved transmembrane proteins modulating K_v channels; however, their possible role in the regulation of memory and age-dependent memory decline are unknown. Here, we show that, in *C. elegans*, *mps-2* is the sole member of the MiRP family that controls exclusively long-term associative memory (LTAM) in AVA neuron. In addition, we demonstrate that *mps-2* also plays a critical role in age-dependent memory decline. In young adult worms, *mps-2* is transcriptionally upregulated by CRH-1/cyclic AMP (cAMP)-response-binding protein (CREB) during LTAM, although the *mps-2* baseline expression is CREB independent and instead, during aging, relies on *nhr-66*, which acts as an age-dependent repressor. Deletion of *nhr-66* or its binding element in the *mps-2* promoter prevents age-dependent transcriptional repression of *mps-2* and memory decline. Finally, MPS-2 acts through the modulation of the K_v2.1/KVS-3 and K_v2.2/KVS-4 heteromeric potassium channels. Altogether, we describe a conserved MPS-2/KVS-3/KVS-4 pathway essential for LTAM and also for a programmed control of physiological age-dependent memory decline.

INTRODUCTION

Voltage-gated, pore-forming potassium (K_v) channels are heteromeric complexes that are active alone; however, ancillary subunits of the evolutionary conserved MinK-related peptide (MiRP)/KCNE gene family modulate their fundamental properties.[1,2] MiRPs (MIRPs or KCNEs) are conserved single-pass transmembrane proteins that associate with K_v channels.[1] In vertebrates, both the K_v channels and the MiRP/KCNE family proteins show a broad expression pattern in various tissues, including heart, uterus, kidney, epithelia, and the nervous system,[1] and have been implicated in excitatory properties of the different cell types. In the brain, K_v channels and their ancillary subunits play an important role in a multitude of neural functions, including the generation and regulation of long-term potentiation (LTP).[1,3]

The *C. elegans* genome encodes four MiRP/KCNE homolog proteins (*mps-1* to *mps-4*) that are all predominantly expressed in the nervous system.[4] Mutant analysis had previously shown that *mps-2* or *mps-3* causes increased sensitivity to Na^+ ions.[4] In addition, MPS-1, -2, and -3 proteins were found to interact with the K^+ ion-channel KVS-1 (orthologous to human K_v4.2) in *C. elegans* and to influence the current characteristics of the ion channel in a heterologous *Xenopus* oocyte system.[4] MPS-1 and KVS-1 also appear to work together in different neurosensory tasks.[5] Finally, MPS-1 also appears to interact with other members of the K_v family, such as KHT-1, the homolog of vertebrate K_v3.1 ion channel, and to control non-associative learning in *C. elegans*.[6] Previously, in a genome-wide microarray study, we have identified *mps-2* as one of approximately 500 genes that were differentially expressed during long-term associative memory (LTAM).[7] Analyzing the identified memory genes, *mps-2* was the only candidate with a dual expression pattern: increase during memory and decrease with aging. *mps-2* is the *C. elegans* ortholog of one member of the MiRP protein family,

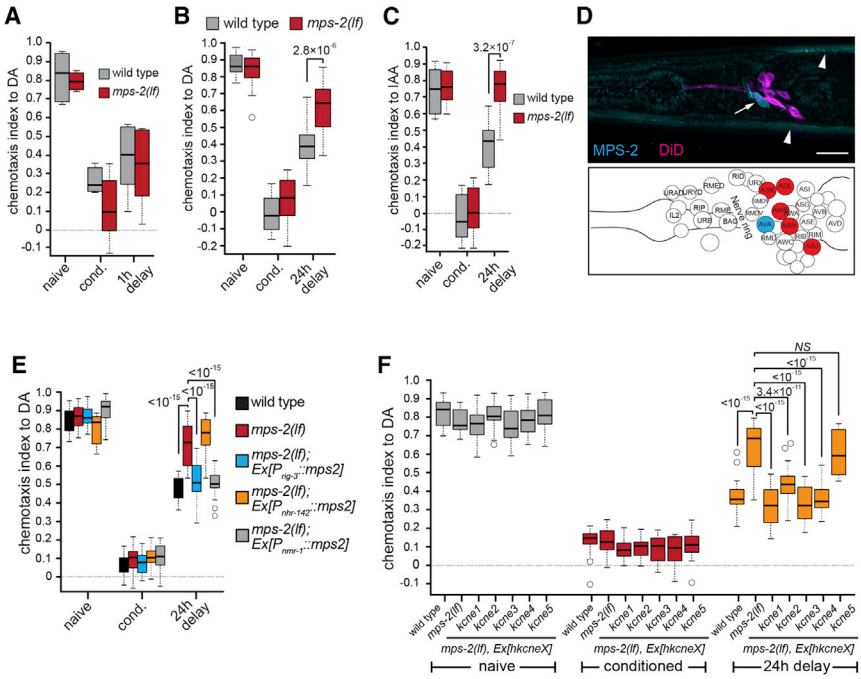

Figure 1. MPS-2 Regulates Long-Term Olfactory Associative Memory in AVA Neuron

(A) Short-term associative memory (STAM) to 0.1% diacetyl (DA) tested in wild-type or *mps-2(lf)* worms.

(B) Wild-type or *mps-2(lf)* worms were tested toward 0.1% DA for LTAM assay.

(C) LTAM to 0.1% isoamyl alcohol (IAA) in wild-type or *mps-2(lf)* worms before (naive), immediately after (cond.), or 24 h following training.

(D) MPS-2 expressing AVA neuron (cyan) in adult brain was compared to the position of DiD-positive amphid cells (red). Arrow points to AVA; arrowheads show expression in body-wall muscle. Scale bar: 10 μm.

(E) Long-term memory of *mps-2(lf)* mutant worms carrying *rig-3* and *nmr-1* for AVA neuron expression or ADF neuron expressing *nhr-162* promoter-driven wild-type *mps-2* gene.

(F) Long-term memory of *mps-2(lf)* mutant worms carrying different human KCNE forms as indicated under the control of worm *mps-2* promoter and 3′ UTR.

Data are visualized with Tukey's boxplots. See Data S1A for detailed statistical information. See also Figure S1.

and its upregulation during LTAM may be directly linked to alteration of neuronal function. In addition, expression of *mps-2* is severely reduced during aging.[8] Thus, *mps-2* represents a unique attractive candidate that might be critical in age-dependent memory decline.

The aging of the brain and associated cognitive decline occurs at multiple layers and at different temporal kinetics, including cell death, plaque formation, synaptic loss, and altered molecular signaling. Over the past decades, the accumulated results suggest that age-dependent cognitive decline is predominantly due to alterations of neuronal morphology and synaptic plasticity. These effects are mainly linked to reduced efficiency of transcription and translation as well as changes in cellular metabolism due to the accumulation of cellular damage and oxidative stress (reviewed in Kandlur et al.[9] and Bettio et al.[10]). Aging rodents, for instance, show reduced hippocampal-dependent recognition, fear, spatial, and associative memories.[11,12] Among others, neuronal-activity-induced genes, like brain-derived neurotrophic factor (BDNF); the cytoskeleton-associated protein (Arc); and most importantly the transcription factor cyclic AMP (cAMP)-response-binding protein (CREB) have been connected to synaptic plasticity changes during the aging of the brain. In *C. elegans*, previous work also found a connection between the KVS-1 ion channel and aging by demonstrating that age-dependent oxidation of KVS-1 may underlie sensory decline.[13] However, it is important to mention that physiological learning and memory decline in *C. elegans* precedes the age-dependent failure of sensation.[14] Therefore, it is unlikely that ROS-mediated oxidation of KVS-1 is directly responsible for memory decline.

Here, we investigated the role of the KCNE family, in particular *mps-2*, in LTAM and in age-dependent memory decline. We could show that, among the MiRP/KCNE homologs in *C. elegans*, only *mps-2* alters selectively aversive long-term memory in young adult worms. Interestingly, expression of human KCNE members in *mps-2(lf)* worms fully rescued the memory defect of the mutant animals. On the other hand, we also demonstrate that *mps-2* plays a critical role in controlling physiological age-dependent memory decline. Using promoter mapping and a yeast one-hybrid (Y1H) screen, we identified *nhr-66* as the transcriptional repressor responsible for the downregulation of *mps-2* expression during aging. Depletion of *nhr-66* or its binding site in the *mps-2* promoter prevents age-dependent transcriptional suppression of *mps-2* and, as a consequence, memory decline. Finally, we also elucidated the molecular pathway, through which MPS-2 exerts its activity, and demonstrated that MPS-2 acts in a tissue-specific manner through the specific modulation of the activity of KVS-3/KVS-4 voltage-gated K^+ ion-channel heteromers. Taken together, our results define the role of KCNE family proteins in the regulation of learning and memory and demonstrate that age-dependent memory decline may be, to some extent, a programmed and actively regulated process.

RESULTS

MPS-2 Is Required for Effective Long-Term Memory

Our previous large-scale expression study identified a set of putative memory-related genes, including *mps-2*, a member of the KCNE protein family. To investigate the impact of the K_v channel ancillary subunit family members on LTAM, we first tested the effect of an *mps-2* knockout mutation on different types of memories in *C. elegans*. Although loss of *mps-2* had no effect on short-term associative memory (STAM) (Figure 1A), LTAM induced by diacetyl, isoamyl alcohol, or salt was impaired (Figures 1B, 1C, and S1A), suggesting that MPS-2 specifically regulates LTAM independent of the sensory input in young adult

worms. In addition, LTAM impairment is specific to *mps-2*, as the deletion of the other members of the MiRP family (*mps-1*, *-3*, and *-4*) showed no effect (Figures S1D–S1F).

MPS-2 Is Transcriptionally Regulated in the AVA Interneuron during LTAM

The genomic region of the *mps-2* locus is very compact, the gene is included in the 3′ UTR of the gene K01A2.4, and in addition, the locus contains several inverted repeats and duplications, including two *mps-2*-like, non-expressed pseudo-genes almost identical to the *mps-2* sequence (Figures S1B and S1C). This complex structure renders the endogenous *mps-2* genomic locus problematic for CRISPR-Cas9-based manipulations, likely due to uncontrollable complex rearrangements during genome editing. To overcome these issues, we analyzed the *mps-2* expression with a reporter plasmid by fusing an 8-kb genomic region of the *mps-2* locus to a C-terminal GFP and *mps-2* 3′ UTR (Figure 4A). MPS-2 was detected throughout development with broad expression in the embryo, including the epidermis, gut, and differentiating neurons (Figures S1G and S1H). During larval development, expression becomes weaker and more restricted and adult worms show MPS-2 expression only in a couple of cells, including body-wall muscle, rectal muscle, somato-intestinal muscle, inconsistently in coelomocytes (Figures 1D, S1I–S1L, and S3A), and robust expression in the AVA neuron (Figures 1D, S1I, S1J, S1L, and S3A), which plays an important role in memory.[15–18] On the other hand, contrary to a previous study, MPS-2 was not detectable in the ADF neuron.[4] To further investigate the cellular focus of *mps-2*, we performed rescue experiments using different neuron-specific promoters fused to the *mps-2* coding region. In accordance with the observed expression pattern of *mps-2*, expression of the gene in AVA under the control of *nmr-1* or *rig-3* promoters rescued the *mps-2(lf)* defect (Figure 1E), while the ADF-specific *nhr-142* was not effective (Figure 1E). Because none of the rescuing promoters is active in body-wall, rectal, or somato-intestinal muscles and the motility of *mps-2(lf)* mutant worms was identical to that of wild-type animals (Figure S1M), it is very unlikely that MPS-2 functions in muscle; it rather affects neuronal activity function during LTAM.

Altogether, the expression pattern in combination with the rescue experiments suggest that *mps-2* acts in the AVA command interneuron during LTAM. Finally, we tested whether *mps-2* function is evolutionary conserved by rescuing the *mps-2(lf)* memory phenotype with the expression of the different human KCNE family members under the control of the worm *mps-2* promoter and 3′ UTR. As expected, several of the human KCNE family members fully rescued the *mps-2(lf)* phenotype despite the difference in primary structure, confirming that the protein function is evolutionary conserved (Figure 1F).

Previously, we identified *mps-2* in a microarray study as a gene that is transcriptionally upregulated during LTAM.[7] Thus, we first investigated the change in global and in AVA-specific quantity of *mps-2* during LTAM. We found that both global *mps-2* mRNA, as well as the protein levels in AVA neuron, increases specifically upon LTAM, but not upon starvation (CS) or exposure to diacetyl (DA) (US) alone (Figures 2A and 2B). Because *mps-2* gene expression is induced during LTAM and CREB plays an essential role in long-term memory in different species,[19] we tested whether *mps-2* transcriptional upregulation during LTAM is CREB dependent. Indeed, we found that loss of the *C. elegans* CREB homolog *crh-1* fully blocked conditioning-induced transcriptional *mps-2* upregulation without influencing the basal *mps-2* expression levels (Figure 2C). Finally, we investigated the temporal requirement for MPS-2 during memory encoding and retrieval. We performed a temporal rescue experiment using heat-shock-driven induction of *mps-2* (*hsp16.2* promoter; *hs::mps-2*) in *mps-2(lf)* mutant worms. The heat-shock treatment increased *mps-2* expression levels for approximately 1 h (Figure 2D). Using this experimental setup, we performed LTAM assays and found that the temporal need for the gene shows a biphasic pattern, with an early and a delayed (2–4 h post-training) requirement of the protein function (Figure 2E) in accordance with the previously reported major gene activation peaks during LTAM,[7] which may coincide with memory encoding and consolidation. Because the MPS/KCNE gene family modulates fundamental properties of voltage-gated potassium channels,[1,2] we measured changes in AVA spontaneous neuronal excitability in naive wild-type animals or in worms 2 h after conditioning, which coincides with maximal increase of MPS-2 levels (Figure 2B) or *mps-2(lf)* mutant worms stably expressing *rig-3* promoter-driven GCaMP6f. Whereas the activation kinetic of AVA neuron remained unaffected upon conditioning or deletion of the *mps-2* gene (Figures 2F and 2G), the loss of *mps-2* decreases inactivation speed of AVA neuron (Figure 2I), suggesting that *mps-2* positively modulates voltage-gated K^+ channel activity of the neuron. In contrast, 2 h after conditioning, when MPS-2 levels peak, we detected a significant increase in inactivation speed (Figure 2H), altogether suggesting that AVA activity may be regulated by alteration of *mps-2* levels.

In summary, our results show that MPS-2 is required and upregulated in AVA during long-term memory and may play a role by increasing activity of K_v channels at specific time points during memory encoding and consolidation rather than during retrieval.

MPS-2 Is a Key Component of a Regulatory Mechanism Controlling Age-Dependent Memory Decline

In order to investigate the putative role of *mps-2* during physiological age-dependent memory decline, we first confirmed that memory decreases in an age-dependent manner in *C. elegans* using different olfactory and gustatory chemotaxis and aversive long-term memory assays (Figures 3A–3C). Interestingly, memory decline always preceded learning, motility (Figure S1M), or sensory impairment (Figure 3A). Furthermore, spontaneous neuronal currents in AVA neuron were affected by age to a similar extent as to what we had observed upon loss of *mps-2* (Figures 1I, 3I, and S2B). Strikingly, we found that the basal expression of *mps-2*, both at the mRNA and at the protein level, rapidly decreased with age within the time frame of the worm early memory decline (Figures 3E and 3H). Furthermore, the drop of *mps-2* levels occurs mainly in AVA, while other tissues seem to express *mps-2* at an even level during aging (Figure S3A). On the other hand, expression levels of other members of the MiRP protein family were unchanged with age (Figures 3D, 3F, and 3G), suggesting that *mps-2* plays a unique dual role in memory consolidation in young animals as well as in age-dependent memory decline.

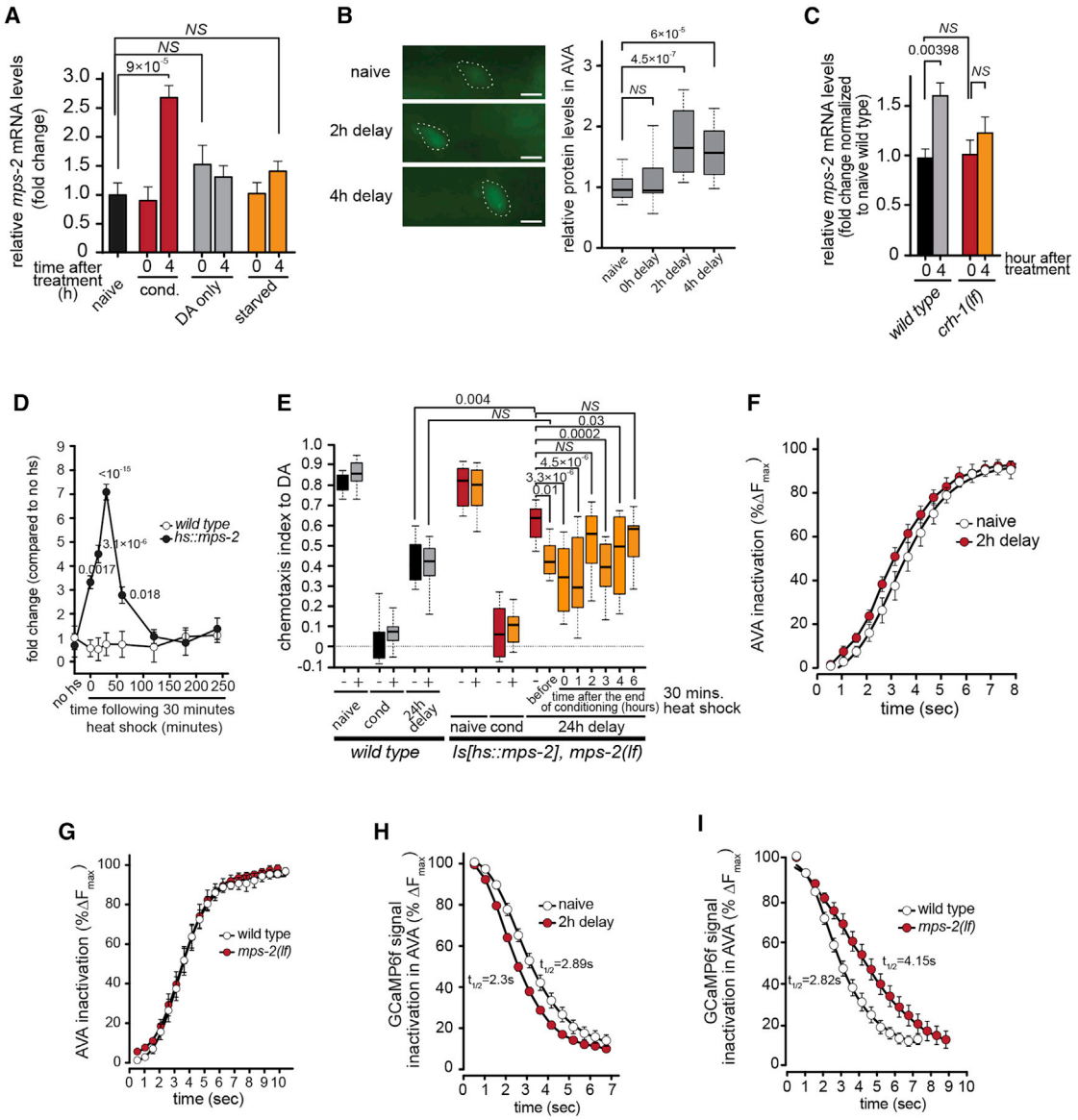

Figure 2. *mps-2* Is Transcriptionally Regulated During LTAM and Modulates AVA Neuron Excitability in Young Adult Worms

(A) *mps-2* RNA levels were measured with qRT-PCR following the indicated treatments and normalized to *tbb-1* and *cdc-42*.

(B) MPS-2::GFP intensity change in AVA (left panels show representative microscopical pictures) at different times after LTAM conditioning and normalized to the naive levels (right part). Scale bar, 5μm.

(C) Wild-type or *crh-1(lf)* worms were conditioned and *mps-2* expression levels were tested with qRT-PCR and normalized to *tbb-1* and *cdc-42*.

(D) Temporal activation profile of $hsp_{16.2}$ promoter-driven *mps-2* upon 30 min heat shock was tested by monitoring *mps-2* transcript levels, as indicated, using real-time qRT-PCR. Expression was normalized to *tbb-2* and presented as fold change of the naive *mps-2* expression levels.

(E) Temporal LTAM rescue of *mps-2(lf)* was tested in a transgenic strain carrying $hsp_{16.2}$ promoter-driven *mps-2* with or without 30 min heat shock as indicated before (naive), immediately after (cond.), or 24 h following training.

(F) Activation dynamics of Ca^{2+} currents in AVA neuron in untrained (naive) young adult wild-type animals or after 2 h recovery following conditioning.

(G) Activation dynamics of Ca^{2+} currents in AVA neuron in wild-type and *mps-2(lf)* mutant animals.

(H) Inactivation dynamics of Ca^{2+} currents in AVA neuron in untrained (naive) young adult wild-type animals or after 2 h recovery following conditioning.

(I) Inactivation dynamics of Ca^{2+} currents in AVA neuron in wild-type and *mps-2(lf)* mutant animals.

Data on (B) and (E) are visualized with Tukey's boxplots; (A), (C), (D), and (F)–(I) show mean ± SE. See Data S1B for detailed statistical information.

In order to elucidate the underlying regulation mechanisms and molecular pathways involving *mps-2* during age-dependent memory decline, we investigated whether the specific drop of MPS-2 expression with age could account for the memory impairment during physiological aging.[20–22] Importantly, *mps-2(lf)* showed normal sensory or motility aging and lifespan (Figures S1M and S2A), suggesting that *mps-2* specifically affects memory decline rather than influencing aging in general. Next,

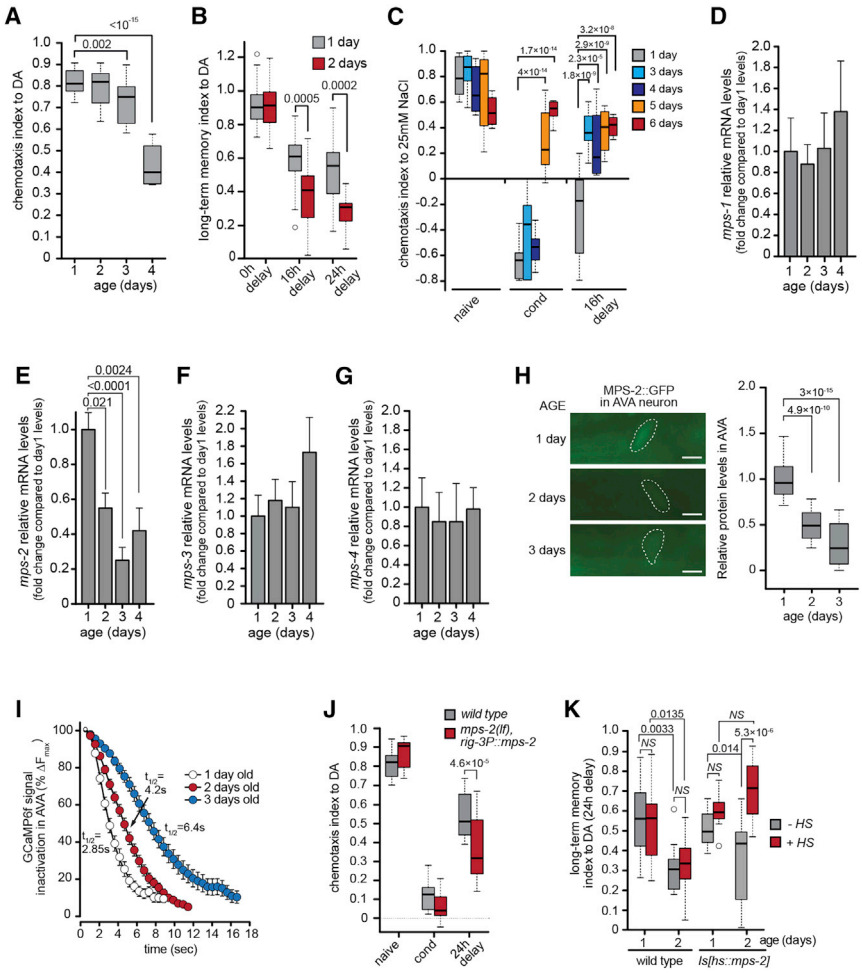

Figure 3. Aging Causes Gradual Impairment of Chemotaxis and LTAM in *C. elegans* through Downregulation of MPS-2 Expression

(A) Age-dependent chemotaxis decline toward DA in wild-type worms.

(B) Age-dependent long-term memory decline in young (1 day) or aged (2 days) wild-type worms. Memory index ($CI_{naive} - CI_{24h\ delay}/CI_{naive}$) was used to normalize for the age-dependent decrease in chemotaxis. Worms were assayed immediately or 16 h or 24 h after conditioning.

(C) Age-dependent learning and long-term memory decline in wild-type animals using salt LTAM assay.

(D–G) RNA levels of (D) *mps-1*, (E) *mps-2*, (F) *mps-3*, and (G) *mps-4* during aging was tested with real-time qRT-PCR; expressions were normalized to *tbb-2* and presented as fold change of the 1-day-old expression levels.

(H) Age-dependent decline of MPS-2::GFP levels in AVA neuron was measured on microscopy images (left part) and quantified by normalizing to the 1-day intensity levels (right part). Scale bar, 5μm.

(I) Inactivation dynamics of spontaneous Ca^{2+} currents in the AVA neuron in wild-type animals during aging as indicated, normalized to the maximal activation signal.

(J) 2-day-old wild-type or AVA-expressing *rig-3*-driven *mps-2* rescued worms (three independent lines) were assayed toward 0.1% DA.

(K) Age-dependent memory decline of LTAM in young (1 day) or aged (2 days) wild-type and *Is[hs::mps-2]* worms with (hs+) or without (hs−) heat shock prior to training. Memory index ($CI_{naive} - CI_{24h\ delay}/CI_{naive}$) 24 h following conditioning is plotted.

Data on (A)–(C), (H), and (J)–(K) are visualized with Tukey's boxplots; (D)–(F) and (I) show mean ± SE. See Data S1C for detailed statistical information. See also Figure S2.

we tested whether an increase in MPS-2 expression in aged animals rescues age-dependent memory decline. Both ectopic expression of MPS-2 in AVA under the control of the constitutive *rig-3* promoter (Figure 3J) as well as the induction of MPS-2 levels prior to conditioning using a heat-shock promoter (Figure 3K) reverted LTAM decline in 2-day-old worms. In contrast, ectopic increase of *mps-2* expression neither affected learning per se nor modified the LTAM in young worms (Figures 3K and S2C), which suggests that ectopic expression of *mps-2* improves memory in an age-dependent manner. Previous findings demonstrated that CREB activity levels decrease in aged rodents and in dementia patients.[23,24] Interestingly, the basal *mps-2* expression levels were not affected in *crh-1(lf)* mutant worms (Figure 1H). Thus, CRH-1 is likely not responsible for the age-dependent downregulation of the basal *mps-2* expression and for the age-dependent memory decline mediated by MPS-2.

NHR-66 Downregulates the Transcription of *mps-2* in an Age-Dependent Manner

In order to identify the promoter element and transcription factors responsible for *mps-2* expression in AVA during aging, we first tested different promoter truncations and identified various promoter elements responsible for different aspects of *mps-2* expression regulation (Figure 4A). Measuring intensities of the GFP reporter fused to different promoter regions, we found a bipartite region required for transcriptional upregulation of *mps-2* expression during LTAM (Figures 4A and 4B). Strikingly, *in silico* prediction defined CRE site containing clusters (1–6 CRE elements in a cluster), which coincided with these identified regions in the *mps-2* promoter (Figure 4A). Thus, we performed *in vitro* electrophoretic mobility shift assay (EMSA) and found that both regions covering these clusters bind recombinant CRH-1 (Figure 4C). In addition, selective reduction of CRH-1 in AVA expressing the previously published *rig-3* promoter-driven GFP hairpin[17] in endogenously tagged crh-1::YPET worms impaired LTAM (Figures 4D and S4B), suggesting that CRH-1 is required for LTAM-induced upregulation of *mps-2* in AVA neuron. Furthermore, deletion of any of the identified promoter elements abolishes LTAM similar to the deletion of the *mps-2* gene (Figure 4A). In summary, we found that the two CRE-element-containing regions are both in conjunction necessary for LTAM-dependent upregulation of MPS-2 in the AVA neuron and for LTAM (Figure 4A). However, these elements neither

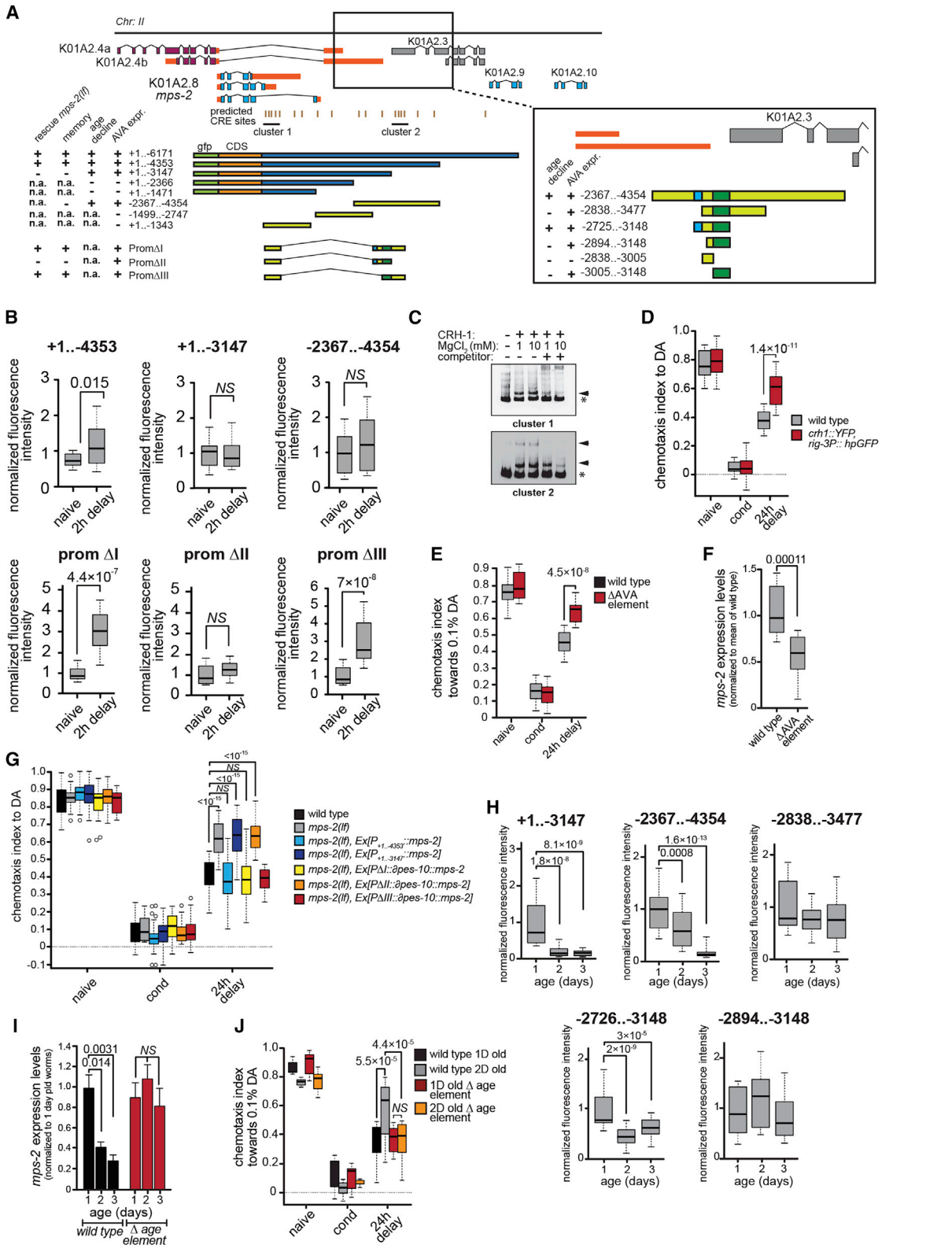

Figure 4. Distinct Elements in *mps-2* Promoter Regulate Transcriptional Control, Tissue-Specific Expression, and Age-Dependent Decline

(A) Schematic representation of the *mps-2* promoter truncations fused to GFP and tested for AVA expression. AVA expression regulatory element is highlighted in green and age-dependent repressor binding site in purple.

(legend continued on next page)

regulate basal *mps-2* expression in AVA neuron nor are required for age-dependent decrease of *mps-2* expression. Adjacent to one of these CRE clusters, we identified a 143-bp region required for basal expression of *mps-2* in AVA (Figures 4F and S3A). Deletion of this second element using CRISPR-Cas9 genome editing impaired LTAM to a similar extent as previously observed for the *mps-2* deletion mutant (Figure 4E). Finally, we performed rescue experiments with different promoter fragments and identified a minimal promoter construct containing only the AVA element together with the two CREB binding clusters that fully rescued the *mps-2(lf)* LTAM phenotype (Figure 4G). Altogether, our results define a minimal sufficient promoter consisting of the two CRE element clusters and the AVA-expression controlling site (Figures 4A and 4G) that is sufficient to reconstitute the temporal and spatial expression profile of the native *mps-2* gene during LTAM.

Although the identified promoter elements are essential for expression in AVA and for the function of *mps-2* during LTAM in young adults (Figures 4F and 4G), they are not responsible for the observed age-dependent decrease of *mps-2* expression in AVA (Figures 3E, 3H, and S3A). Therefore, to identify the age-dependent repressor element, we performed additional truncations and identified a third, 110-bp sequence, adjacent to the AVA expression element that is necessary for the downregulation of *mps-2* expression during aging (Figures 4A and 4H). Deletion of this element is sufficient to fully block age-dependent memory decline and the decrease of *mps-2* transcription with age (Figures 4H–4J), which suggests that a transcriptional repressor may actively suppress *mps-2* transcription during aging. In summary, the promoter mapping revealed three important regions in the *mps-2* promoter. The first is responsible for the basal expression of the gene in AVA neuron, a second composed of a bipartite region mediates transcriptional upregulation during LTAM and finally, a third element controls repression of basal *mps-2* levels during aging (Figure 4A).

To identify the putative age-dependent repressor, we used the 110-bp age-regulatory element as bait in a Y1H screen and identified the nuclear hormone receptor, *nhr-66*, as the transcription factor interacting with this DNA element (Figures 5A and 5B). The *C. elegans* NHR-66 shows similarity to the vertebrate *Hnf4a* and retinoic acid receptor (RXR/RAR) transcription factors. In worms, depletion of *nhr-66* fully suppressed age-dependent memory decline and the change of *mps-2* expression with age (Figures 5C and 5D), similar to the deletion of the *nhr-66* DNA-binding element in the *mps-2* promoter (Figures 4I and 4J). In adult *C. elegans*, *nhr-66* is broadly expressed, including hypodermis, gut, muscle, and neuronal cells of the ventral nerve chord, head, and tail ganglia (Figure 5F). In the head ganglion, several sensory and interneurons, including AVA, express NHR-66 (Figure 5G). Interestingly, global *nhr-66* expression was not altered with age (Figure 5E), and we could not observe any difference in NHR-66 abundance during aging in AVA neuron (data not shown), pointing to a controlled regulation of the transcription factor activity rather than to changes of expression levels. In summary, our results demonstrate that age-dependent memory decline is controlled and transcriptional repression of MPS-2 by NHR-66 likely results in a reduced K_v ion-channel activity and decrease in neuronal activity of specific neurons.

MPS-2 Specifically Acts through KVS-3 and KVS-4 Potassium Channels

The *C. elegans* genome encodes 72 potassium channels, ten of which belong to the voltage-gated channel subfamily, three to the KQT, and two genes to the Eag-like subfamilies.[25] In order to identify which of these channels are modulated by MPS-2, we first performed a targeted RNAi screen and identified KVS-3 and KVS-4,[26] the *C. elegans* $K_v2.1$ and $K_v2.2$ homologs, respectively (Figures 6A–6C). Depletion of either of the two genes impaired LTAM to a similar extent as the loss of *mps-2*. Therefore, we generated deletion mutants for the candidate genes using CRISPR-Cas9, confirmed their memory phenotype, and checked for a genetic interaction of the two channels. Deletion of either of the K^+ channels strongly impaired LTAM similar to the double mutant, which suggests that KVS-3 and KVS-4 may function together and form a heteromeric complex during memory formation (Figure 6D).[27] Finally, we tested the genetic interaction of the ion channels with MPS-2. Although overexpression of *mps-2* using *hs::mps-2* rescues the memory defect of the *mps-2(lf)* mutants, induced increase of MPS-2 together with simultaneous reduction of the MPS-2 effector potassium channels should attenuate each other and result in failure of LTAM rescue. Indeed, double mutants carrying *Is [hs::mps-2]* with either *kvs-3(lf)* or *kvs-4(lf)* showed impaired LTAM memory irrespective of the ectopic induction of *mps-2* (Figure 6E).

(B) Promoter fragments as indicated were fused to GFP, tested for fluorescence intensity, and normalized to the mean of naive expression in naive or 2 h post-conditioned animals.
(C) CRH-1 binding to CRE-element-containing clusters was tested with EMSA with or without an unlabeled competitor DNA fragment and different Mg^{2+} ion concentrations as indicated.
(D) Wild-type or AVA-specific *crh-1* RNAi (*crh-1::YFP; rig-3P::hpGFP* worms; two independent lines) were assayed for LTAM toward 0.1% DA.
(E) Wild type or worms carrying deletion of the AVA expression regulatory element were assayed for LTAM toward 0.1% DA.
(F) *mps-2* RNA levels were measured with real-time qRT-PCR in wild-type and AVA-regulator-element deletion strain. Expression levels were normalized to *tbb-1*.
(G) LTAM rescue of *mps-2(lf)* was tested in transgenic strains carrying different promoter truncations (see also A) driving the wild-type *mps-2* by monitoring attraction to DA before (naive) or immediately (cond.) or 24 h following training.
(H) Promoter fragments as indicated (see also A) were fused to GFP, and fluorescence intensity was measured at different ages and normalized to the mean of 1 day expression.
(I) *mps-2* RNA levels were measured with real-time qRT-PCR in wild-type and age-dependent regulatory element deletion strain during aging. Expression values were normalized to *tbb-1*.
(J) Age-dependent memory decline of LTAM in young (1 day) or aged (2 days) wild-type worms or age-dependent regulatory element deletion strain.
Data are visualized with Tukey's boxplot; (I) shows mean ± SE. See Data S1D for detailed statistical information. See also Figure S3.

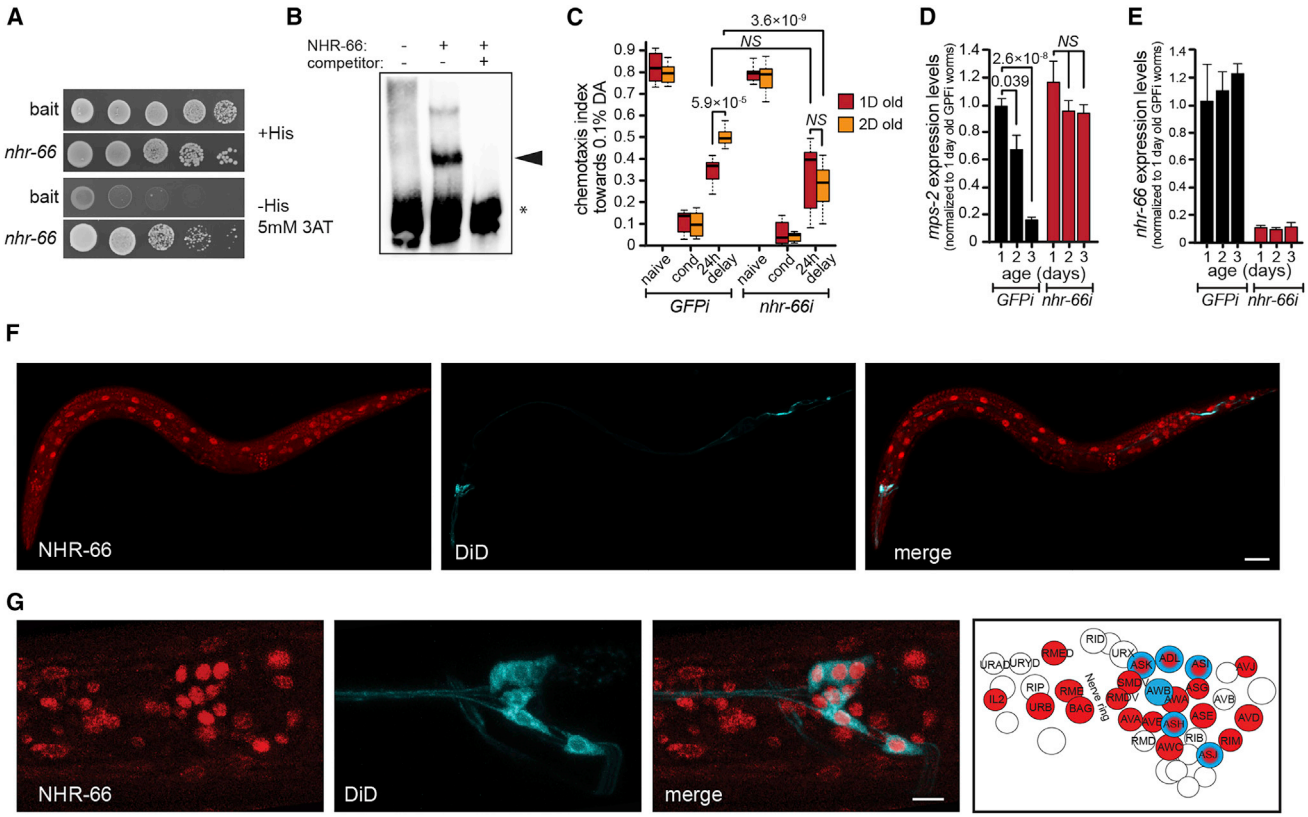

Figure 5. NHR-66 Is a Repressor of *mps-2* Expression during Age-Dependent Memory Decline

(A) Yeast growth assay on His^+ or His^- plates supplemented with 5 mM 3-AT selection of the isolated Y1H clone carrying the 110-bp *mps-2* promoter fragment covering the age-dependent regulatory element as bait and *nhr-66* as prey.

(B) Bacterially expressed NHR-66 binding to *mps-2* age-dependent regulatory element was tested with EMSA.

(C) Age-dependent memory decline of LTAM in young (1 day) or aged (2 days) control (*gfpi*) or *nhr-66* RNAi-treated worms (*nhr-66i*).

(D) *mps-2* RNA levels were measured with qRT-PCR in RNAi-treated worms as indicated and normalized to *tbb-1*.

(E) *nhr-66* RNA levels were measured with real-time qRT-PCR in RNAi-treated worms as indicated and normalized to *tbb-1*.

(F and G) Endogenously tagged NHR-66 (red) expression pattern in young adults (F) or in the head neurons (G). DiD-stained amphid cells were used as reference points (cyan). Scale bar, 50 μm (F) and 5 μm (G).

Data in (C) are visualized with Tukey's boxplot; (D) and (E) show mean ± SE. See Data S1E for detailed statistical information.

MPS-2 Forms *In Vivo* Heteromers in AVA Neuron with KVS-3 and KVS-4 Potassium Channels

Our genetic results strongly suggested that MPS-2 associates and modulates the activity of KVS-3/Kv2.1 and KVS-4/Kv2.2 K_v channels. In order to confirm the interaction between MPS-2 and KVS-3/4 proteins *in vivo*, we used the split-GFP system[28] to study the pairwise association between MPS-2 and the different ion-channel proteins. We first tested the overall expression pattern of KVS-3 or KVS-4 in the nervous system of the worm. Hence, we co-expressed KVS-3 or KVS-4 fused to GFP_{11} together with $GFP_{1–10}$ in an operon with mCherry to confirm expression under the control of the pan-neuronal *rgef-1* promoter. As shown in Figure S3, both KVS-3 and KVS-4 are broadly expressed in the *C. elegans* nervous system, including the AVA interneuron. Next, we tested pairwise interaction between MPS-2, KVS-3, and KVS-4 and also the homo- or heteromeric complex formation of the two ion channels. We found that both KVS-3 and KVS-4 form a homomeric complex (Figures 7A and 7B) in a subset of the ion-channel-expressing neurons (see also Figures S4A–S4D). In addition, we found that KVS-3 and KVS-4 also form hetero-oligomers that are detectable in several neurons, including the AVA interneuron (Figure 7C). Surprisingly, the subcellular distribution of the KVS-3/KVS-4 heteromer in AVA differs from the localization observed in other neuronal cells. The heteromeric ion-channel complex shows uniform membrane localization in all neuronal cells except in AVA, where the KVS-3/KVS-4 complex is in punctae representing specific subcellular clusters. In addition, we found that MPS-2 is in complex with both KVS-3 and KVS-4 exclusively in the AVA neuron, forming clusters at the membrane (Figures 7D and 7E) that are strikingly similar to the KVS-3/KVS-4 subcellular pattern (Figures 7D and 7E). Because MPS-2 is transcriptionally upregulated during LTAM, we wondered whether the newly synthesized MPS-2 protein gets inserted into the KVS ion-channel complexes in order to modulate their activity. Thus, we analyzed the abundance of the MPS-2/KVS complexes by measuring the splitGFP signal

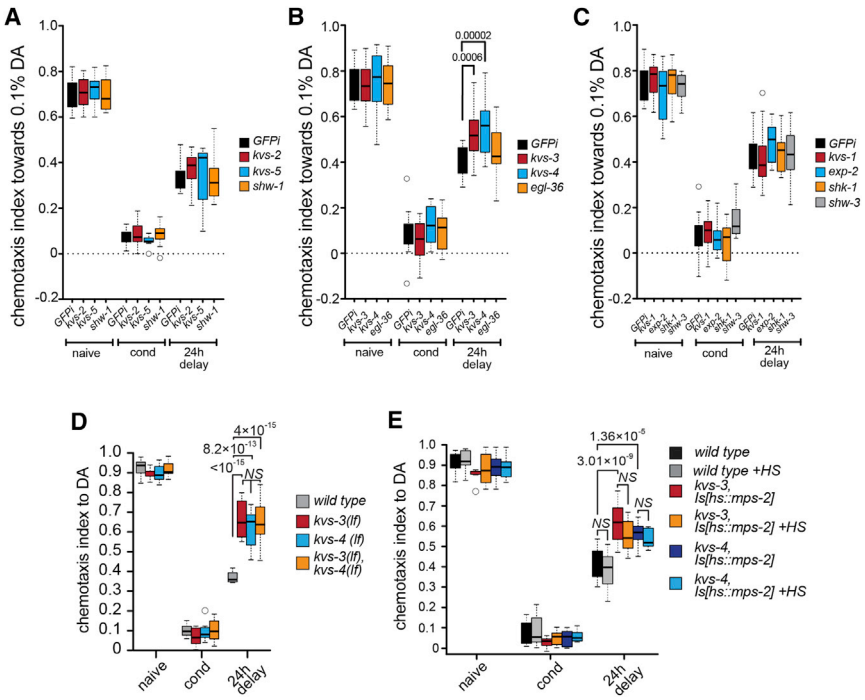

Figure 6. MPS-2 Genetically Acts through KVS-3 and KVS-4 Voltage-Gated K^+ Ion Channels

(A–C) RNAi silencing of the different voltage-gated ion channels in RNAi hypersensitive strain was performed by feeding animals from early L3 animals until adulthood in presence of double-stranded RNA (dsRNA)-containing bacteria as indicated. Young adult animals were assayed for LTAM toward 0.1% DA.

(D) Single mutant phenotypes and genetic interaction between *kvs-3(lf)* and *kvs-4(lf)* voltage-gated potassium channels were tested with LTAM assay toward DA.

(E) Genetic interaction between *kvs-3(lf)*, *kvs-4(lf)*, and *mps-2* overexpression (*hs::mps-2*) using heat-shock induction during training was tested for LTAM.

Data are visualized with Tukey's boxplot. See Data S1F for detailed statistical information.

intensity change upon LTAM. In line with our hypothesis, the total splitGFP signal significantly increased both for MPS-2/KVS-3 and also for MPS-2/KVS-4 complexes (Figures 7F and 7G). Besides the increase in the total amount of the MPS-2/KVS complex upon LTAM, we also investigated the change in the subcellular distribution of the MPS-2/KVS-3 complex during memory induction. In order to account for differences in the intensities, we quantified the ratio of the GFP signal in clusters over the total fluorescence in AVA. As shown in Figure 7H, LTAM induced a significant shift of MPS-2/KVS-3 complexes out of the clusters. In summary, our genetic and *in vivo* microscopy results suggest that, in AVA, a trimeric complex composed of MPS-2, KVS-3, and KVS-4 dynamically changes its composition and subcellular localization during LTAM, which likely increases AVA excitability and regulates memory consolidation. On the other hand, reduced levels of MPS-2 during aging interfere with formation of the trimeric complex and decrease memory in general.

DISCUSSION

In summary, we identified a molecular pathway that controls LTAM by modulating the excitability of the AVA neuron in young adult worms. In addition, the core component of this pathway is also involved in the age-dependent memory decline by an active age-dependent transcriptional repression mechanism. Furthermore, we identified *nhr-66* as the repressor that controls *mps-2* expression during aging, which suggests that age-dependent memory decline is not simply the consequence of a passive gradual deterioration of neuronal signaling[29–31] but at least in part a controlled, regulated event.

MPS-2 was previously identified in a genome-wide, memory-related gene expression screen,[7] and here, we demonstrate that MPS-2 is the sole member of the MPS protein family that regulates long-term memory in our assays but has no impact on chemosensation, motility, or short-term memory. In addition, a temporal rescue experiment shows that MPS-2 likely acts on memory formation and consolidation rather than on retrieval. The *C. elegans* MPS genes are the orthologs of vertebrate KCNEs, and despite the clear structural differences between worm and human proteins, the function of the MPS-2/KCNE is conserved. Interestingly, based on the rescue experiments, several human KCNE forms can replace the function of MPS-2 in worms. This suggests that human KCNEs differ rather in their expression pattern than in their biological role.

In addition, we demonstrated that the effect of *mps-2* is independent of the sensory input, which is in line with the observed expression pattern of the gene product in the AVA interneuron. Furthermore, our rescue experiments demonstrate that MPS-2 in AVA is sufficient to completely rescue the *mps-2* loss-of-function phenotype. In accord with previous findings, AVA seems to play a central role in memory.[15–17] Therefore, the correct modulation of its activity through changes in voltage-gated, ion-channel activities may be essential for memory establishment, consolidation, and retrieval.

Strikingly, we found that MPS-2 is also involved in age-dependent memory decline. This role is, however, likely independent of CREB because the baseline expression of MPS-2, which decreases with age, is not affected by the deletion of CRH-1. To elucidate the nature of the *mps-2* repressor, we identified the *mps-2* promoter region mediating age-dependent transcriptional downregulation. Using a Y1H screen, we identified the interacting transcription factor, *nhr-66*, responsible for the age-dependent transcriptional repression of *mps-2*, but not required for the basal expression of the gene. The *C. elegans* genome encodes 284 different nuclear hormone receptors, most of them unexplored, including NHR-66. So far, NHR-66 was identified as the NHR-49 binding partner that regulates genes in the sphingolipid and lipid remodeling pathway; however, a microarray study suggests that NHR-66 can act independently of the

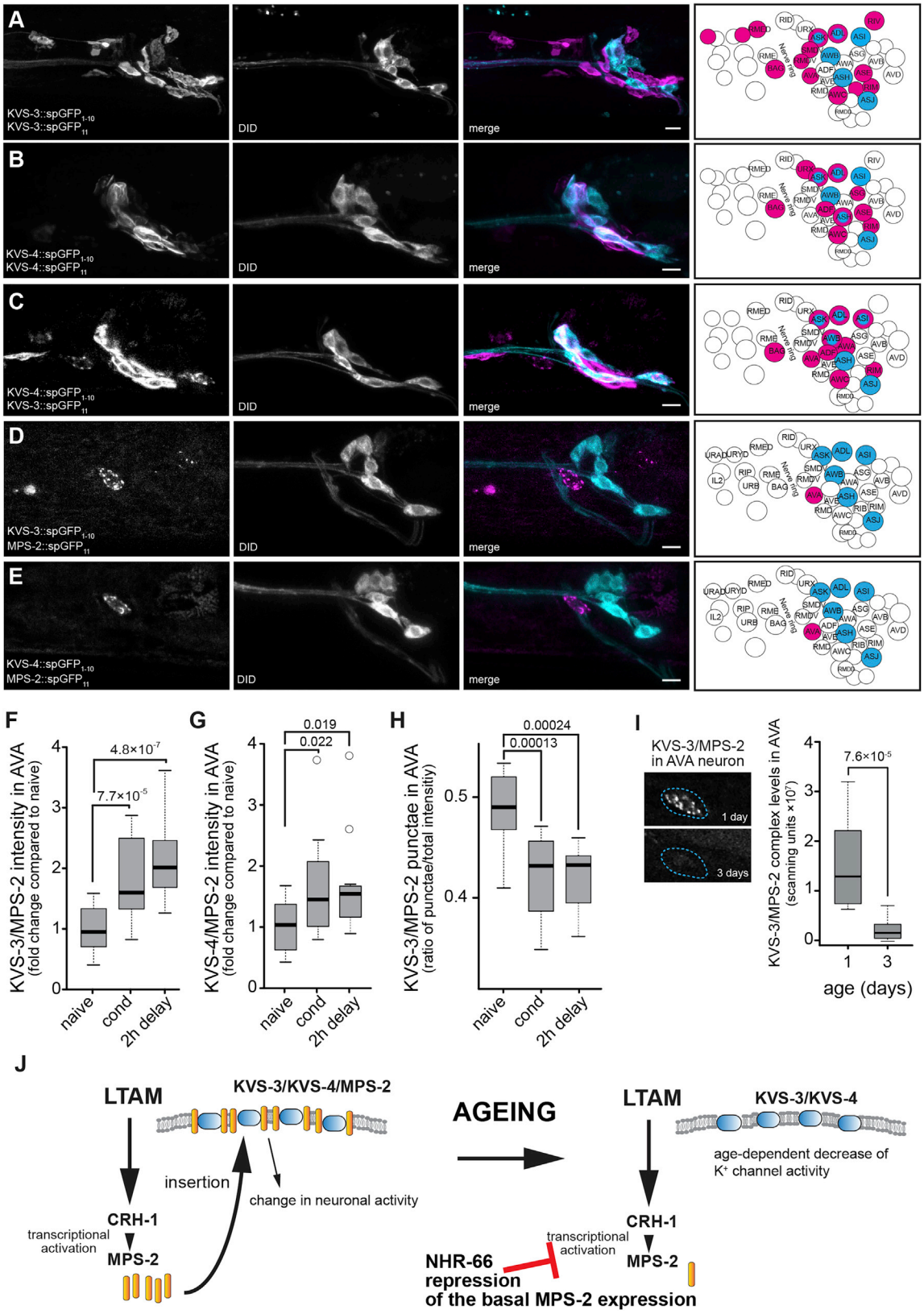

(legend on next page)

NHR-49 to regulate unique pathways.[32] At the sequence level, NHR-66 shows similarity to *Hnf4a* and RXR/RAR vertebrate transcription factors, both genes being expressed in the vertebrate nervous system. Interestingly, HNF4A is linked to Parkinson's disease[33] and dendritic abnormalities observed in Alzheimer's disease.[34] RXR/RAR on the other hand has been reported to have an important role in hippocampus-dependent memory;[35] thus, the NHR-66-mediated repression of MPS-2 could represent an evolutionary conserved regulated mechanism underlying physiological age-dependent memory decline.

We also found that MPS-2 exerts its effect likely by modulating KVS-3 and KVS-4 activity, the nematode homologs of Kv2.1 and Kv2.2 proteins, respectively. Kv2.1 and Kv2.2 are likely the predominant subunits of K_v channel in mammalian brain, including the hippocampus.[36] In cells, the different K_v channel subunits are assembled in tetrameric complexes *in vivo*, and the formation of such heteromers increases the variety of channel complexes and K^+ conductances dramatically. It was previously shown that Kv2 subunits are in complex with Kv5, Kv6, Kv8, and Kv9,[37–39] and initial studies argued against the formation of functional Kv2.1/2.2 ion-channel heteromers. This was based on the different subcellular distribution of the two proteins and functionality tests in overexpression of the subunits in heterologous HEK293 cells.[40–43] In contrast, the work of Kihira et al.[27] demonstrated that Kv2.1 and Kv2.2, indeed, colocalize in large clusters, physically interact, and form heteromeric complexes in cortical pyramidal neurons. However, the formation and biological role of Kv2.1/2.2 complex remains controversial and unexplored. In addition, Kv2.1 activity is further modulated by insertion of MiNK/MiRP proteins into the functional ion-channel complex, which usually reduces Kv2.1 activation kinetics in cardiac tissue or in the brain.[44,45] Interestingly, our data demonstrate that, besides homomeric complexes, a heteromeric KVS-3 and KVS-4 complex forms *in vivo* in AVA neurons in the *C. elegans* nervous system. In addition, both ion-channel subunits are also in complex with MPS-2, suggesting the presence of a K^+ channel complex consisting of KVS-3, KVS-4, and MPS-2. Furthermore, our genetic results suggest that this heteromeric complex is essential for correct memory formation in young adult animals. Thus, we demonstrate here the *in vivo* formation of KVS-3/Kv2.1 KVS-4/Kv2.2 heteromeric complex and demonstrate that this specific ion-channel oligomer plays an essential role during memory. Strikingly, the KVS-3/KVS-4/MPS-2 complex localizes in large clusters in AVA similar to previous observations in vertebrate cells for Kv2.1.[43] The role of these clusters is currently under debate, but a dynamic, activity-dependent relocation in or out of these clusters likely plays a role in the proper functioning of the ion channels.[46] Previous results propose that K_v complexes in the clusters are inactive and, therefore, a switch to the "soluble" form is required for activation.[47,48] In accord with this hypothesis, our results point to a shift of KVS-3/MPS-2 complexes from a "clustered" to a soluble state during LTAM. Altogether, our data show an essential role of MPS-2 specifically in LTAM, and we demonstrate that MPS-2 forms a complex and likely acts in the modulation of activity specifically of KVS-3/KVS-4 heteromeric K_v channel complex in order to maintain memory (Figure 7J).

In summary, our results describe a molecular pathway in which the core element plays a dual role; on one hand, it is required for the maintenance of memory in young animals, and on the other hand, it is also responsible for physiological age-dependent memory decline. Furthermore, our data imply the existence of an active age-dependent repression mechanism that controls reduction of memory performance during aging.

STAR★METHODS

Detailed methods are provided in the online version of this paper and include the following:

- KEY RESOURCES TABLE
- RESOURCE AVAILABILITY
  - Lead Contact
  - Materials Availability
  - Data and Code Availability
- EXPERIMENTAL MODEL AND SUBJECT DETAILS
  - Worm strains and maintenance
- METHOD DETAILS
  - Molecular biology and plasmid constructs
  - Microinjection and generation of transgenic worms
  - RNA interference
  - Locomotory rate assay
  - Olfactory memory assays
  - Salt memory assay
  - Real-time RT-qPCR
  - Electrophoresis mobility shift assay (EMSA)
  - Fluorescent microscopy
  - Ca^{2+} activity measurements
  - Yeast one-hybrid screen
  - Worm survival
- QUANTIFICATION AND STATISTICAL ANALYSIS

SUPPLEMENTAL INFORMATION

Supplemental Information can be found online at https://doi.org/10.1016/j.cub.2020.10.069.

Figure 7. KVS-3, KVS-4, and MPS-2 Form Complexes *In Vivo*, which Are Regulated during LTAM

(A–C) Homomer of (A) KVS-3, (B) KVS-4, or (C) heteromer between KVS-3 and KVS-4 distribution visualized *in vivo* with splitGFP in worm head neurons.

(D and E) Heteromerization of MPS-2 with (D) KVS-3 or with (E) KVS-4 in head neurons.

(F and G) KVS-3/MPS-2 (F) or KVS-4/MPS-2 (G) heteromer complex level changes during LTAM. Intensities of splitGFP signal were measured upon treatment as indicated and normalized to the mean of naive levels.

(H) Quantification of the distribution of diffuse/clustered KVS-3/MPS-2 complex ratio upon LTAM.

(I) Distribution of KVS-3/MPS-2 complexes in the AVA neuron during aging was measured on z-projected confocal images (left panels) and plotted as scanned intensities (right panel).

(J) Model of the molecular pathway that regulates LTAM through *mps-2* and voltage-gated potassium channels in AVA neurons in young animals and during aging.

See Data S1G for detailed statistical information. See also Figure S4. Scale bar for (A–E), 5 μm.

ACKNOWLEDGMENTS

We are grateful to Anne Spang for generously sharing reagents and instruments. We would also like to thank the Caenorhabditis Genetic Centre (supported by NIH Office of Research Infrastructure Programs P40OD010440) for providing nematode strains. The work was supported by the Swiss National Science Foundation (SNSF) grant (31003A_178937) to A.S.

AUTHOR CONTRIBUTIONS

B.G.F., V.G.G., C.H., A.A., K.T., and F.P. conducted the experiments; D.d.Q. and A.P. evaluated the data and wrote the manuscript; and A.S. planned, designed, and conducted the experiments, evaluated the data, interpreted the results, and wrote the manuscript.

DECLARATION OF INTERESTS

The authors declare no competing interests.

Received: June 15, 2020
Revised: September 14, 2020
Accepted: October 21, 2020
Published: November 30, 2020

REFERENCES

1. McCrossan, Z.A., and Abbott, G.W. (2004). The MinK-related peptides. Neuropharmacology *47*, 787–821.
2. Abbott, G.W. (2016). KCNE1 and KCNE3: The yin and yang of voltage-gated K(+) channel regulation. Gene *576*, 1–13.
3. Lewis, A., McCrossan, Z.A., and Abbott, G.W. (2004). MinK, MiRP1, and MiRP2 diversify Kv3.1 and Kv3.2 potassium channel gating. J. Biol. Chem. *279*, 7884–7892.
4. Park, K.H., Hernandez, L., Cai, S.Q., Wang, Y., and Sesti, F. (2005). A family of K+ channel ancillary subunits regulate taste sensitivity in Caenorhabditis elegans. J. Biol. Chem. *280*, 21893–21899.
5. Bianchi, L., Kwok, S.M., Driscoll, M., and Sesti, F. (2003). A potassium channel-MiRP complex controls neurosensory function in Caenorhabditis elegans. J. Biol. Chem. *278*, 12415–12424.
6. Cai, S.Q., Wang, Y., Park, K.H., Tong, X., Pan, Z., and Sesti, F. (2009). Auto-phosphorylation of a voltage-gated K+ channel controls non-associative learning. EMBO J. *28*, 1601–1611.
7. Freytag, V., Probst, S., Hadziselimovic, N., Boglari, C., Hauser, Y., Peter, F., Gabor Fenyves, B., Milnik, A., Demougin, P., Vukojevic, V., et al. (2017). Genome-wide temporal expression profiling in *Caenorhabditis elegans* identifies a core gene set related to long-term memory. J. Neurosci. *37*, 6661–6672.
8. Youngman, M.J., Rogers, Z.N., and Kim, D.H. (2011). A decline in p38 MAPK signaling underlies immunosenescence in Caenorhabditis elegans. PLoS Genet. *7*, e1002082.
9. Kandlur, A., Satyamoorthy, K., and Gangadharan, G. (2020). Oxidative stress in cognitive and epigenetic aging: a retrospective glance. Front. Mol. Neurosci. *13*, 41.
10. Bettio, L.E.B., Rajendran, L., and Gil-Mohapel, J. (2017). The effects of aging in the hippocampus and cognitive decline. Neurosci. Biobehav. Rev. *79*, 66–86.
11. Singh, P., and Thakur, M.K. (2014). Reduced recognition memory is correlated with decrease in DNA methyltransferase1 and increase in histone deacetylase2 protein expression in old male mice. Biogerontology *15*, 339–346.
12. Peleg, S., Sananbenesi, F., Zovoilis, A., Burkhardt, S., Bahari-Javan, S., Agis-Balboa, R.C., Cota, P., Wittnam, J.L., Gogol-Doering, A., Opitz, L., et al. (2010). Altered histone acetylation is associated with age-dependent memory impairment in mice. Science *328*, 753–756.
13. Cai, S.Q., and Sesti, F. (2009). Oxidation of a potassium channel causes progressive sensory function loss during aging. Nat. Neurosci. *12*, 611–617.
14. Kauffman, A.L., Ashraf, J.M., Corces-Zimmerman, M.R., Landis, J.N., and Murphy, C.T. (2010). Insulin signaling and dietary restriction differentially influence the decline of learning and memory with age. PLoS Biol. *8*, e1000372.
15. Hadziselimovic, N., Vukojevic, V., Peter, F., Milnik, A., Fastenrath, M., Fenyves, B.G., Hieber, P., Demougin, P., Vogler, C., de Quervain, D.J., et al. (2014). Forgetting is regulated via Musashi-mediated translational control of the Arp2/3 complex. Cell *156*, 1153–1166.
16. Stetak, A., Hörndli, F., Maricq, A.V., van den Heuvel, S., and Hajnal, A. (2009). Neuron-specific regulation of associative learning and memory by MAGI-1 in C. elegans. PLoS ONE *4*, e6019.
17. Vukojevic, V., Gschwind, L., Vogler, C., Demougin, P., de Quervain, D.J., Papassotiropoulos, A., and Stetak, A. (2012). A role for α-adducin (ADD-1) in nematode and human memory. EMBO J. *31*, 1453–1466.
18. Ha, H.I., Hendricks, M., Shen, Y., Gabel, C.V., Fang-Yen, C., Qin, Y., Colón-Ramos, D., Shen, K., Samuel, A.D., and Zhang, Y. (2010). Functional organization of a neural network for aversive olfactory learning in Caenorhabditis elegans. Neuron *68*, 1173–1186.
19. Silva, A.J., Kogan, J.H., Frankland, P.W., and Kida, S. (1998). CREB and memory. Annu. Rev. Neurosci. *21*, 127–148.
20. Kaletsky, R., Lakhina, V., Arey, R., Williams, A., Landis, J., Ashraf, J., and Murphy, C.T. (2016). The C. elegans adult neuronal IIS/FOXO transcriptome reveals adult phenotype regulators. Nature *529*, 92–96.
21. Stein, G.M., and Murphy, C.T. (2012). The intersection of aging, longevity pathways, and learning and memory in C. elegans. Front. Genet. *3*, 259.
22. Kauffman, A., Parsons, L., Stein, G., Wills, A., Kaletsky, R., and Murphy, C. (2011). C. elegans positive butanone learning, short-term, and long-term associative memory assays. J. Vis. Exp. 2490.
23. Bach, M.E., Barad, M., Son, H., Zhuo, M., Lu, Y.F., Shih, R., Mansuy, I., Hawkins, R.D., and Kandel, E.R. (1999). Age-related defects in spatial memory are correlated with defects in the late phase of hippocampal long-term potentiation in vitro and are attenuated by drugs that enhance the cAMP signaling pathway. Proc. Natl. Acad. Sci. USA *96*, 5280–5285.
24. Kudo, K., Wati, H., Qiao, C., Arita, J., and Kanba, S. (2005). Age-related disturbance of memory and CREB phosphorylation in CA1 area of hippocampus of rats. Brain Res. *1054*, 30–37.
25. Bargmann, C.I. (1998). Neurobiology of the Caenorhabditis elegans genome. Science *282*, 2028–2033.
26. Zhou, X., Zeng, J., Ouyang, C., Luo, Q., Yu, M., Yang, Z., Wang, H., Shen, K., and Shi, A. (2016). A novel bipartite UNC-101/AP-1 μ1 binding signal mediates KVS-4/Kv2.1 somatodendritic distribution in Caenorhabditis elegans. FEBS Lett. *590*, 76–92.
27. Kihira, Y., Hermanstyne, T.O., and Misonou, H. (2010). Formation of heteromeric Kv2 channels in mammalian brain neurons. J. Biol. Chem. *285*, 15048–15055.
28. Cabantous, S., Terwilliger, T.C., and Waldo, G.S. (2005). Protein tagging and detection with engineered self-assembling fragments of green fluorescent protein. Nat. Biotechnol. *23*, 102–107.
29. Craik, F.I., and Bialystok, E. (2006). Cognition through the lifespan: mechanisms of change. Trends Cogn. Sci. *10*, 131–138.
30. Konar, A., Singh, P., and Thakur, M.K. (2016). Age-associated cognitive decline: insights into molecular switches and recovery avenues. Aging Dis. *7*, 121–129.
31. Sesti, F. (2016). Oxidation of K(+) channels in aging and neurodegeneration. Aging Dis. *7*, 130–135.
32. Pathare, P.P., Lin, A., Bornfeldt, K.E., Taubert, S., and Van Gilst, M.R. (2012). Coordinate regulation of lipid metabolism by novel nuclear receptor partnerships. PLoS Genet. *8*, e1002645.
33. Fernández-Santiago, R., Carballo-Carbajal, I., Castellano, G., Torrent, R., Richaud, Y., Sánchez-Danés, A., Vilarrasa-Blasi, R., Sánchez-Pla, A., Mosquera, J.L., Soriano, J., et al. (2015). Aberrant epigenome in iPSC-

derived dopaminergic neurons from Parkinson's disease patients. EMBO Mol. Med. *7*, 1529–1546.

34. Liu, D., Tang, H., Li, X.Y., Deng, M.F., Wei, N., Wang, X., Zhou, Y.F., Wang, D.Q., Fu, P., Wang, J.Z., et al. (2017). Targeting the HDAC2/HNF-4A/miR-101b/AMPK pathway rescues tauopathy and dendritic abnormalities in Alzheimer's disease. Mol. Ther. *25*, 752–764.
35. Nomoto, M., Takeda, Y., Uchida, S., Mitsuda, K., Enomoto, H., Saito, K., Choi, T., Watabe, A.M., Kobayashi, S., Masushige, S., et al. (2012). Dysfunction of the RAR/RXR signaling pathway in the forebrain impairs hippocampal memory and synaptic plasticity. Mol. Brain *5*, 8.
36. Murakoshi, H., and Trimmer, J.S. (1999). Identification of the Kv2.1 K+ channel as a major component of the delayed rectifier K+ current in rat hippocampal neurons. J. Neurosci. *19*, 1728–1735.
37. Kramer, J.W., Post, M.A., Brown, A.M., and Kirsch, G.E. (1998). Modulation of potassium channel gating by coexpression of Kv2.1 with regulatory Kv5.1 or Kv6.1 alpha-subunits. Am. J. Physiol. *274*, C1501–C1510.
38. Post, M.A., Kirsch, G.E., and Brown, A.M. (1996). Kv2.1 and electrically silent Kv6.1 potassium channel subunits combine and express a novel current. FEBS Lett. *399*, 177–182.
39. Salinas, M., de Weille, J., Guillemare, E., Lazdunski, M., and Hugnot, J.P. (1997). Modes of regulation of shab K+ channel activity by the Kv8.1 subunit. J. Biol. Chem. *272*, 8774–8780.
40. Guan, D., Tkatch, T., Surmeier, D.J., Armstrong, W.E., and Foehring, R.C. (2007). Kv2 subunits underlie slowly inactivating potassium current in rat neocortical pyramidal neurons. J. Physiol. *581*, 941–960.
41. Hwang, P.M., Fotuhi, M., Bredt, D.S., Cunningham, A.M., and Snyder, S.H. (1993). Contrasting immunohistochemical localizations in rat brain of two novel K+ channels of the Shab subfamily. J. Neurosci. *13*, 1569–1576.
42. Lim, S.T., Antonucci, D.E., Scannevin, R.H., and Trimmer, J.S. (2000). A novel targeting signal for proximal clustering of the Kv2.1 K+ channel in hippocampal neurons. Neuron *25*, 385–397.
43. Trimmer, J.S. (1991). Immunological identification and characterization of a delayed rectifier K+ channel polypeptide in rat brain. Proc. Natl. Acad. Sci. USA *88*, 10764–10768.
44. McCrossan, Z.A., Lewis, A., Panaghie, G., Jordan, P.N., Christini, D.J., Lerner, D.J., and Abbott, G.W. (2003). MinK-related peptide 2 modulates Kv2.1 and Kv3.1 potassium channels in mammalian brain. J. Neurosci. *23*, 8077–8091.
45. McCrossan, Z.A., Roepke, T.K., Lewis, A., Panaghie, G., and Abbott, G.W. (2009). Regulation of the Kv2.1 potassium channel by MinK and MiRP1. J. Membr. Biol. *228*, 1–14.
46. O'Connell, K.M., Rolig, A.S., Whitesell, J.D., and Tamkun, M.M. (2006). Kv2.1 potassium channels are retained within dynamic cell surface microdomains that are defined by a perimeter fence. J. Neurosci. *26*, 9609–9618.
47. Fox, P.D., Loftus, R.J., and Tamkun, M.M. (2013). Regulation of Kv2.1 K(+) conductance by cell surface channel density. J. Neurosci. *33*, 1259–1270.
48. O'Connell, K.M., and Tamkun, M.M. (2005). Targeting of voltage-gated potassium channel isoforms to distinct cell surface microdomains. J. Cell Sci. *118*, 2155–2166.
49. Dickinson, D.J., Pani, A.M., Heppert, J.K., Higgins, C.D., and Goldstein, B. (2015). Streamlined genome engineering with a self-excising drug selection cassette. Genetics *200*, 1035–1049.
50. Maduro, M., and Pilgrim, D. (1995). Identification and cloning of unc-119, a gene expressed in the Caenorhabditis elegans nervous system. Genetics *141*, 977–988.
51. Feinberg, E.H., Vanhoven, M.K., Bendesky, A., Wang, G., Fetter, R.D., Shen, K., and Bargmann, C.I. (2008). GFP reconstitution across synaptic partners (GRASP) defines cell contacts and synapses in living nervous systems. Neuron *57*, 353–363.
52. Schneider, C.A., Rasband, W.S., and Eliceiri, K.W. (2012). NIH Image to ImageJ: 25 years of image analysis. Nat. Methods *9*, 671–675.
53. Brenner, S. (1974). The genetics of Caenorhabditis elegans. Genetics *77*, 71–94.
54. Kim, H., Ishidate, T., Ghanta, K.S., Seth, M., Conte, D., Jr., Shirayama, M., and Mello, C.C. (2014). A co-CRISPR strategy for efficient genome editing in Caenorhabditis elegans. Genetics *197*, 1069–1080.
55. Mohri, A., Kodama, E., Kimura, K.D., Koike, M., Mizuno, T., and Mori, I. (2005). Genetic control of temperature preference in the nematode Caenorhabditis elegans. Genetics *169*, 1437–1450.
56. Sawin, E.R., Ranganathan, R., and Horvitz, H.R. (2000). C. elegans locomotory rate is modulated by the environment through a dopaminergic pathway and by experience through a serotonergic pathway. Neuron *26*, 619–631.
57. Nuttley, W.M., Atkinson-Leadbeater, K.P., and Van Der Kooy, D. (2002). Serotonin mediates food-odor associative learning in the nematode Caenorhabditiselegans. Proc. Natl. Acad. Sci. USA *99*, 12449–12454.
58. Wicks, S.R., de Vries, C.J., van Luenen, H.G., and Plasterk, R.H. (2000). CHE-3, a cytosolic dynein heavy chain, is required for sensory cilia structure and function in Caenorhabditis elegans. Dev. Biol. *221*, 295–307.

STAR★METHODS

KEY RESOURCES TABLE

REAGENT or RESOURCE	SOURCE	IDENTIFIER
Chemicals, Peptides, and Recombinant Proteins		
2, 3-Butanedione	Sigma Aldrich	11038
NaN_3	Sigma Aldrich	71290
Q5 Taq polymerase	New England Biolabs	M0491S
NEBuilder HiFi assembly kit	New England Biolabs	E2621L
Q5 Taq polymerase	New England Biolabs	M0491S
IPTG	Applichem	A1008.0005
Proteinase K	Roche	3115879001
Maxima first strand cDNA synthesis kit	Thermo Fisher Scientific	15273796
SyBr fast kit	Kapa Biosystems	KK4605
Ni-NTA Resin	QIAGEN	1018244
dI-dC	Thermo Fisher Scientific	20148E
Nitran Supercharge nylon membrane	Schleicher & Schuell	10416296
Chemiluminescent nucleic acid detection module	Thermo Fisher Scientific	89880
polystyrene microsphere bead solution	Polyscience	00876
Lithium-acetate	Sigma Aldrich	62395
Salmon sperm DNA	Sigma Aldrich	D1626
3-Amino-1,2,4-triazole	Sigma Aldrich	A8056
Experimental Models: Organisms/Strains		
C. elegans: mps-2(ok1631)	Caenorhabditis Genetics Center	Strain: RB1431
C. elegans: utrIs13[hsp16.2p::mps-2::mps-2 3'UTR; sur-5p::dsred], mps-2(ok1631)	This Paper	Strain: STA212
C. elegans: mps-2(ok1631); utrEx77[nmr-1p::mps-2::mps-2 3'UTR; sur-5p::dsRed]	This Paper	Strains: STA282-STA284
C. elegans: mps-2(ok1631); utrEx78[rig-3p::mps-2::mps-2 3'UTR; sur-5p::dsRed]	This Paper	Strains: STA285-STA286
C. elegans: mps-2(ok1631); utrEx81[nhr-142p::mps-2::mps-2 3'UTR; sur-5p::dsRed]	This Paper	Strains: STA293-STA294
C. elegans: unc-119(ed3); utrEx82[mps-2p::mps-2::GFP::mps-2 3'UTR; unc-119(+)]	This Paper	Strains: STA310-STA311
C. elegans: unc-119(ed3); utrEx84[mps-2p$_{+1..-1471}$:: mps-2::GFP::mps-2 3'UTR; unc-119+]	This Paper	Strains: STA328-STA329
C. elegans: unc-119(ed3); utrEx86[mps-2p$_{+1..-2366}$:: mps-2::GFP::mps-2 3'UTR; unc-119+]	This Paper	Strain: STA330
C. elegans: unc-119(ed3); utrEx87[mps-2p$_{-2367..-4354}$:: ∂pes-10::NLS::GFP::unc-54 3'UTR; unc-119+]	This Paper	Strains: STA331-STA333
C. elegans: unc-119(ed3); utrEx88[mps-2p$_{-2894..-3148}$:: ∂pes-10::NLS::GFP::unc-54 3'UTR; unc-119+]	This Paper	Strains: STA344-STA345
C. elegans: unc-119(ed3); utrEx93[mps-2p$_{-2838..-3477}$:: ∂pes10::NLS::GFP::unc-54 3'UTR; unc-119+]	This Paper	Strain: STA356
C. elegans: unc-119(ed3); utrEx94[mps-2p$_{+1..3147}$::mps-2::NLS::GFP::unc-54 3'UTR; unc-119+]	This Paper	Strain: STA361
C. elegans: unc-119(ed3); utrEx95[mps-2p$_{-2725..-3148}$:: ∂pes-10::NLS::GFP::unc-54 3'UTR; unc-119+]	This Paper	Strains: STA362-STA363
C. elegans: unc-119(ed3); utrEx96[mps-2p$_{-2894..-3148}$:: ∂pes-10::NLS::GFP::unc-54 3'UTR; unc-119+]	This Paper	Strain: STA365

(*Continued on next page*)

Continued

REAGENT or RESOURCE	SOURCE	IDENTIFIER
C. elegans: unc-119(ed3); utrEx97[mps-2p ΔI::mps-2::GFP::mps-2 3'UTR; unc-119+]	This Paper	Strain: STA366
C. elegans: unc-119(ed3); utrEx98[mps-2p ΔII::mps-2::GFP::mps-2 3'UTR; unc-119+]	This Paper	Strain: STA368
C. elegans: unc-119(ed3); utrEx99[mps-2p ΔIII::mps-2::GFP::mps-2 3'UTR; unc-119+]	This Paper	Strain: STA367
C. elegans: kvs-3(utr27)	This Paper	Strain: STA378
C. elegans: kvs-4(utr31)	This Paper	Strain: STA379
C. elegans: kvs-4(utr31); kvs-3(utr27)	This Paper	Strain: STA383
C. elegans: utrIs13[hsp16.2p::mps-2::unc-54 3'UTR; sur-5p::dsRed]; kvs-4(utr31)	This Paper	Strain: STA382
C. elegans: utrIs13[hsp16.2p::mps-2::unc-54 3'UTR; sur-5p::dsRed]; kvs-3(utr27)	This Paper	Strain: STA384
C. elegans: mps-1(ok1376)	Caenorhabditis Genetics Center	Strain: VC955
C. elegans: mps-4(ok3285)	Caenorhabditis Genetics Center	Strain: VC2574
C. elegans: mps-3(ok2045)	Caenorhabditis Genetics Center	Strain: RB1655
C. elegans: crh-1(utr20[crh-1::2xYFP::3xFLAG])	This Paper	Strain: STA323
C. elegans: crh-1(utr20[crh-1::;2xYFP::3xFLAG]); utrEx103[rig-3p::hpGFP; myo-2p::mCherry]	This Paper	Strains: STA404-STA405
C. elegans: mps-2(utr36[DelAVA element])	This Paper	Strain: STA387
C. elegans: mps-2(utr38[DelAge element])	This Paper	Strain: STA389
C. elegans: mps-2(ok1631); utrEx100[mps-2p$_{+1..-4353}$::mps-2; myo-2p::mCherry]	This Paper	Strains: STA395-STA397
C. elegans: mps-2(ok1631); utrEx101[mps-2p$_{+1..-3147}$::mps-2; myo-2p::mCherry]	This Paper	Strains: STA398-STA400
C. elegans: mps-2(ok1631); utrEx102[mps-2p ΔI::mps-2; myo-2p::mCherry]	This Paper	Strains: STA401-STA403
C. elegans: mps-2(ok1631); utrEx104[mps-2p ΔII::mps-2; myo-2p::mCherry]	This Paper	Strains: STA410-STA412
C. elegans: mps-2(ok1631); utrEx105[mps-2p ΔIII::mps-2; myo-2p::mCherry]	This Paper	Strains: STA413-STA415
C. elegans: utrEx113[kvs-3::spGFP$_{1-10}$; kvs-3::spGFP$_{11}$; myo-2p::mCherry]	This Paper	Strain: STA478
C. elegans: utrEx114[mps-2::spGFP$_{11}$; kvs-3::spGFP$_{1-10}$; myo-2p::mCherry]	This Paper	Strain: STA498
C. elegans: utrEx116[kvs-3::spGFP$_{11}$; rgef-1p::spGFP$_{1-10}$::SL2::mCherry]	This Paper	Strain: STA507
C. elegans: utrEx117[kvs-3::spGFP$_{11}$; kvs-4::spGFP$_{1-10}$; myo-2p::mCherry]	This Paper	Strain: STA513
C. elegans: utrEx119[kvs-4::spGFP$_{11}$; kvs-4::spGFP$_{1-10}$; myo-2p::mCherry]	This Paper	Strain: STA518
C. elegans: utrEx120[kvs-4::spGFP$_{11}$; rgef-1p::spGFP$_{1-10}$::SL2::mCherry]	This Paper	Strain: STA520
C. elegans: utrEx121[rig-3p::hKCNE1::unc-54 3'UTR; myo-2p::mCherry]	This Paper	Strains: STA531-STA532
C. elegans: utrEx122[rig-3p::hKCNE2::unc-54 3'UTR; myo-2p::mCherry]	This Paper	Strains: STA533-STA534
C. elegans: utrEx123[rig-3p::hKCNE3::unc-54 3'UTR; myo-2p::mCherry]	This Paper	Strains: STA535-STA536
C. elegans: utrEx124[rig-3p::hKCNE4::unc-54 3'UTR; myo-2p::mCherry]	This Paper	Strains: STA537-STA538
C. elegans: utrEx125[rig-3p::hKCNE5::unc-54 3'UTR; myo-2p::mCherry]	This Paper	Strains: STA539-STA540

(*Continued on next page*)

Continued

REAGENT or RESOURCE	SOURCE	IDENTIFIER
C. elegans: nhr-66(utr47[2xYpet::SEC::AID::3xFLAG])	This Paper	Strain: STA494
C. elegans: utrIs25[rig-3p::GCaMP6f; unc-119+]	This Paper	Strain: STA357
C. elegans: mps-2(ok1631); utrIs25[rig-3p::GCaMP6f; unc-119+].	This Paper	Strain: STA359
C. elegans: unc-119(ed3)	Caenorhabditis Genetics Center	Strain: HT1593
C. elegans: sid-1(pk3321) uIs69[unc-119p::sid-1(+); myo-2p::cherry]	Caenorhabditis Genetics Center	Strain: TU3401
Oligonucleotides		
Primers for qPCR, see Table S1	This Paper	N/A
Primers for CRISPR/Cas9, see Table S1	This Paper	N/A
Recombinant DNA		
pGEMT easy hsp16.2p::mps-2::mps-2 3'UTR	This Paper	N/A
sur-5p::dsRed	This Paper	N/A
pCFJ90	[49]	Addgene Plasmid #19327
pCFJ104	[49]	Addgene Plasmid #19328
pDD162	[49]	Addgene Plasmid #47549
pDD162ΔCas9	This Paper	N/A
pDD283::2xYPET	This Paper	N/A
Punc-119+	[50]	pDP#MM016b
L4440	Gift from Andrew Fire	Addgene Plasmid #1654
pGEMT easy nmr-1p::mps-2::mps-2 3'UTR	This Paper	N/A
pGEMT easy rig-3p::mps-2::mps-2 3'UTR;	This Paper	N/A
pGEMT easy nhr-142p::mps-2::mps-2 3'UTR	This Paper	N/A
pBS KS+ 6kb mps-2p::mps-2::GFP::mps-2 3'UTR	This Paper	N/A
pBS KS+ mps-2p$_{+1..-1471}$::mps-2::GFP::mps-2 3'UTR	This Paper	N/A
pBS KS+ mps-2p$_{+1..-2366}$::mps-2::GFP::mps-2 3'UTR	This Paper	N/A
pBS KS+ mps-2p$_{-2367..-4354}$::∂pes-10::NLS::YFP::unc-54 3'UTR	This Paper	N/A
pBS KS+ mps-2p$_{-2894..-3148}$::∂pes-10::NLS::YFP::unc-54 3'UTR	This Paper	N/A
pBS KS+ mps-2p$_{-2838..-3477}$::∂pes10::NLS::GFP::unc-54 3'UTR	This Paper	N/A
pBS KS+ mps-2p$_{+1..-3147}$::mps-2::GFP::unc-54 3'UTR	This Paper	N/A
pBS KS+ mps-2p$_{-2725..-3148}$::∂pes-10::NLS::GFP::unc-54 3'UTR	This Paper	N/A
pBS KS+ mps-2p ΔI::mps-2::GFP::mps-2 3'UTR	This Paper	N/A
pBS KS+ mps-2p ΔII::mps-2::GFP::mps-2 3'UTR	This Paper	N/A
pBS KS+ mps-2p ΔIII::mps-2::GFP::mps-2 3'UTR	This Paper	N/A
pDD283::crh-1::2xYPET	This Paper	N/A
rig-3p::hpGFP	[17]	N/A
pBS KS+ kvs-3::spGFP1-10	This Paper	N/A
pflp-18::NGL-1::spGFP11	[51]	Addgene Plasmid #65828
punc-4::NGL-1::spGFP1-	[51]	Addgene Plasmid #65827
pBS KS+ kvs-3::spGFP11	This Paper	N/A
L4440-kvs-2	This Paper	N/A
L4440-kvs-5	This Paper	N/A
L4440-shw-1	This Paper	N/A
pET14b-nhr-66	This Paper	N/A
pET14b-crh-1	This Paper	N/A
pGEMT easy mps-2::spGFP11	This Paper	N/A

(*Continued on next page*)

Continued

REAGENT or RESOURCE	SOURCE	IDENTIFIER
pGEMT easy rgef-1p::spGFP1-10::SL2::mCherry	This Paper	N/A
pBS KS+ kvs-4::spGFP1-10	This Paper	N/A
pBS KS+ kvs-4::spGFP11	This Paper	N/A
pGEMT easy rig-3p::hKCNE1::unc-54 3'UTR	This Paper	N/A
pGEMT easy rig-3p::hKCNE2::unc-54 3'UTR	This Paper	N/A
pGEMT easy rig-3p::hKCNE3::unc-54 3'UTR	This Paper	N/A
pGEMT easy rig-3p::hKCNE4::unc-54 3'UTR	This Paper	N/A
pGEMT easy rig-3p::hKCNE5::unc-54 3'UTR	This Paper	N/A
pDD283::nhr-66::2xYPET::AID	This Paper	N/A
pDD162ΔCas9-nhr-66	This Paper	N/A
pDD162ΔCas9-crh-1	This Paper	N/A
pDD162ΔCas9-kvs-3	This Paper	N/A
pDD162ΔCas9-kvs-4	This Paper	N/A
peft-3::Cas9::NLS::tbb-2 UTR	[49]	Addgene Plasmid #46168
Software and Algorithms		
ImageJ	[52]	https://imagej.nih.gov/ij/
Prism 7.0b	GraphPad	https://www.graphpad.com/scientific-software/prism/

RESOURCE AVAILABILITY

Lead Contact

Further information and requests for resources and reagents should be directed to and will be fulfilled by the Lead Contact, Attila Stetak (a.stetak@unibas.ch).

Materials Availability

Plasmids and strains are available upon request.

Data and Code Availability

This study did not generate/analyze datasets or codes.

EXPERIMENTAL MODEL AND SUBJECT DETAILS

Worm strains and maintenance

C. elegans strains were maintained at 15, 20 or 25°C on standard NGM plates and fed with OP50 as described previously[53]. The *C. elegans* Bristol strain, variety N2, was used as the wild-type reference strain in all experiments. The experiments were performed with synchronized worm population. Gravid adult worms were washed with M9 and bleached using alkaline hypochlorite solution (0.5M NaOH, 5% HOCl). Eggs were allowed to hatch on non-seeded CTX agar plates overnight at 20°C.The synchronized L1 worms were grown on NGM-OP50 plates to adulthood at 15, 20 or 25°C and experiments were conducted at RT in acclimatized rooms. Alleles and transgenes used in this study are listed in the Key Resources Table.

METHOD DETAILS

Molecular biology and plasmid constructs

The different promoter and gene fragments were amplified with Q5 high fidelity Taq polymerase from N2 genomic DNA and cloned with NEBuilder HiFi assembly kit (New England BioLabs, Ipswich, MA). sgRNA sequence was inserted into a modified pDD162 plasmid lacking Cas9 with Q5 mutagenesis kit (New England BioLabs, Ipswich, MA) according to manufacturer's protocol. For RNAi clones missing in the Ahringer RNAi library a 500-1000 bp genomic piece of the target gene was inserted into L4440 NcoI site (for primers used, see Table S1). All plasmid constructs were confirmed with sequencing. Plasmids used in this work are listed in Key Resources Table. Further information on the construct sequence, primers used are available upon request.

Microinjection and generation of transgenic worms

Transgenic lines were generated by injecting the indicated DNA constructs at a concentration of 50-100 ng/μl together with transformation marker into syncytial gonad arms of young adult worms. The transformation markers *sur-5p::dsred* and *unc-119+* were

used at 10 ng/μl, *myo-3p::mcherry* at 5 ng/μl and *myo-2p::mcherry* at 2.5 ng/μl concentrations. Extrachromosomal arrays were integrated with UV and obtained lines were outcrossed 4 times following integration. CRISPR/Cas9 genome editing for YFP integration was performed with self-excising drug cassette (SEC)[49] and mutagenesis or small deletions with co-CRISPR strategy[54] using plasmids encoding the specific sgRNAs and repair oligos introducing stop codon and frameshift at the NT end of the target genes together with *unc-22* coCRISPR marker. For all CRISPR/Cas9 injections, sgRNA coding plasmid was injected at 50 ng/μl together with 25 ng/μl *eft-3p::Cas9::NLS::tbb-2 3'UTR* plasmid with markers as described. Primers used are listed in Table S1.

RNA interference

dsRNA silencing with feeding of the different ion-channel clones and *nhr-66* were done in RNA hypersensitive *sid-1(pk3321) uIs69 [unc119p::sid-1(+); myo-2p::mcherry]* strain. For control, HT115 bacteria carrying dsRNA against GFP (*gfpi*) was used. All other bacterial clones expressing dsRNA for the different target genes were from the Ahringer RNAi library or cloned in L4440 vector as described above. All clones were confirmed with sequencing. For the RNAi silencing, synchronized L1 larvae were first transferred on NGM plates seeded with HT115 bacteria containing the different dsRNA expressing plasmids without induction with IPTG and worms were grown until mid-L3 stage at 20°C. Next, worms were transferred on fresh NGM plates seeded with HT115 bacteria containing the corresponding dsRNA and expression of dsRNA was induced with 5mM IPTG for 2 days at RT prior the transfer. Worms were further grown on the induced dsRNA containing RNAi plates in presence of 5 mM IPTG until adulthood at 15°C. The RNAi treated adult worms were tested for olfactory long-term memory or for gene expression using RT-qPCR as described below. RNA silencing of *crh-1* in AVA was done as described previously by combining YFP-tagged *crh-1* CRISPR line with *rig-3* promoter driven GFP hairpin construct[17]. Gene silencing efficiency of the hairpin construct was monitored using microscopical quantification of CRH-1::YFP signal intensities in AVA (Figure 4B).

Locomotory rate assay

Motility of worms was performed on a bacterial lawn as described[55,56]. Briefly, synchronized L1 worms were grown under uncrowded conditions until adulthood with abundant food and worms were transferred on 6 cm assay plates seeded with OP50 for testing. Two minutes following transfer, the number of body bends of the animals from each strain and time point was counted for 1 min.

Olfactory memory assays

Attraction to the olfactory cue diacetyl (2,3-Butanenione) (DA) was tested in a population of well-fed, synchronized adults. Animals were washed three times with CTX buffer (5 mM KH_2PO_4/K_2HPO_4 pH 6.0, 1 mM $CaCl_2$, and 1 mM $MgSO_4$) and 50–200 worms were placed in the middle of a 10-cm CTX testing plate (5 mM KH_2PO_4/K_2HPO_4 pH = 6.0, 1 mM $CaCl_2$, 1 mM $MgSO_4$, 2% agar). Worms were given a choice for 1 h between a spot of attractant diluted in ethanol with 20 mM sodium-azide and a reference spot with ethanol and sodium-azide. After 1 h test, worms within 1 cm radius of the attractant or reference spot, and the total number of worms on the plate were counted separately. The distribution of the worms was visualized with the chemotaxis index (Chemotaxis Index = $\frac{\text{worms at compound spot} - \text{worms at reference spot}}{\text{total amount of worms on plate}}$). In the case of memory assays with aged animals, memory index (CI_{naive}-$CI_{xh\ delay}$/CI_{naive}) was used to normalize for the age-dependent reduction in chemotaxis. Short-term memory was performed as described earlier[57]. Briefly, well-fed young adult worms were exposed for 1 h to starvation in the presence of 2 μL undiluted chemoattractant (DA) and their attraction to DA was tested prior (naive), directly after (conditioned) and following a 1-h rest in absence of DA and food (1h delay). Olfactory long-term associative memory (LTAM) conditioning was performed as previously described[17]. Briefly, well-fed young adult worms were exposed for two rounds of starvation in the presence of 2 μL undiluted chemoattractant (DA) for 1h with 30 min rest between trainings. After the spaced training, worms were kept on NGM plates in the presence of abundant food for 24 h and tested for their chemotaxis after the recovery phase[17]. For each experiment a fraction of the population was tested prior (naive), immediately following (conditioned) or 24 h after training (24h delay). For all conditions 3 independent test plates were used and the assay repeated at least three times on different days.

Salt memory assay

Chemotaxis to NaCl was tested on four quadrant Petri plates (Falcon X plate, Becton Dickinson Labware, Franklin Lakes, NJ) as described previously[58]. Briefly, pairs of opposite quadrants were filled with CTX agar supplemented with or without 25 mM NaCl. Quadrants were connected immediately prior the assay with thin layer of agar. For the assay a population of well-fed adult worms was washed with CTX buffer and 50-100 worms were placed at the intersection of the quadrants and the distribution of the animals was determined after 10 min. For LTAM conditioning we used spaced training involving three rounds of 2 h starvation in presence of NaCl with a 30 min resting phase between trainings. After the spaced training, worms were kept on NGM plates in the presence of abundant food for the recovery phase. For each experiment a fraction of the population was tested prior (naive), immediately following (conditioned) or 24 h after training (24h delay).

Real-time RT-qPCR

RNA expression levels were measured from synchronized adult worms. For each sample 20 animals were collected in 4μl worm lysis buffer (50 mM KCl, 10 mM Tris-HCl pH 8.2, 2.5 mM $MgCl_2$, 0.45% NP-40, 0.45% Tween-20, 0.01% gelatin) supplemented with 60μg/ml proteinase K and digested for 1 h at 50°C followed by 10 min at 95°C. The samples were processed immediately with Maxima first strand cDNA synthesis kit (Thermo Fisher Scientific, Waltham, MA) according to the manufacturer's recommendation. Real-time

qPCR was performed with gene specific primers (Table S1) using SyBr fast kit (Kapa Biosystems, Wilmington, MA) in a Rotor Gene-6000 instrument (Corbett Research, Mortlake, New South Wales, Australia). Expression levels were normalized to *tba-1*, *act-1* and *cdc-42* expression as indicated. Fold differences were calculated using the $\Delta\Delta C_t$ method.

Electrophoresis mobility shift assay (EMSA)

6xHis-tagged NHR-66 protein was expressed in BL21 DE3 bacteria and induction was performed with 0.2 mM IPTG O/N at 18°C. Cells were lysed under native condition and the expressed protein was purified on Ni-NTA Resin (QIAGEN, Hilden, Germany) according to manufacturer's recommendation. Biotinylated DNA of the *mps-2* age-dependent regulatory element was generated by annealing complementary pairs of synthesized biotinylated oligonucleotides (Microsynth AG, Balgach, Switzerland). The electrophoresis mobility assay reaction was performed on ice for 15 min in 20 μl reaction volume containing 1x reaction buffer (15 mM HEPES pH8.0, 80 mM NaCl, 15 mM KCl, 20 μM EDTA, 10 mM DTT, 3% glycerol), 1 μg dI-dC, 10 mM $MgCl_2$, 2 μg purified His-tag protein, 5 nM biotinylated probe and 1μM non-biotinylated probe as competitor. Protein-DNA complexes were separated on 6 or 10% acrylamide TBE gels, transferred onto Nitran Supercharge nylon membrane (Whatman, Maidstone, UK), UV crosslinked, and labeled probes were detected with Chemiluminescent nucleic acid detection module (Thermo Fisher Scientific, Waltham, MA) according to the manufacturer's protocol.

Fluorescent microscopy

GFP, YFP, mCherry, DiD or splitGFP were detected with a Zeiss Axio Observer LSM 880 inverted confocal microscope with 25x/0.8 or 63x/1.4 oil Plan APO objective. For DiD staining, worms were incubated with 10 μg/ml DiD in M9 for 3 h at RT with constant agitation in dark. Animals were mounted on 3% agarose pads were immobilized with 20 mM NaN_3 and the different fluorophores were detected with sequential scanning using the appropriate lasers and filter sets. The different GFP reporter intensities were recorded with a Zeiss Axio Observer Z1 inverted microscope. For the recording, illumination was reduced to 10% to minimize bleaching. Fluorescent signal intensities were analyzed with FIJI and for all expression analyses the total GFP intensity was measured following global background subtraction. The measured raw intensities were normalized to the mean of the naive, untreated or 1 day old adult signals according to the different experiments. Split GFP clusters were analyzed with FIJI using particle analysis tool after manual setting the threshold. All identified particle intensities were summed up. For the ratio analysis, the total intensity was measured in AVA cells that were manually selected.

Ca^{2+} activity measurements

For Ca^{2+} measurements in AVA neuron, synchronized adult animals of the indicated genotypes or age carrying an integrated *rig-3* promoter driven GCaMP6f sensor (strain: *utrIs25[rig-3p::GCaMP6f; unc-119+]*) were mounted on 5% agarose pads and worms were immobilized in 4μl of 100μm polystyrene microsphere bead solution (Polysciences GmbH, Germany). The effect of conditioning was tested in young adult wild-type animals that were conditioned with two rounds of starvation in the presence of 2 μL undiluted chemoattractant (DA) for 1h with 30 min rest between trainings identical for LTAM assay. After conditioning, worms were kept on NGM plates with abundant food for 2 h identical to experiments testing *mps-2* expression. Conditioning and recovery were initiated at different time-points and only 2 animals for each conditioning set were recorded to keep the 2 h recovery phase constant. GCaMP6f signal intensity was measured on a Zeiss Axio Observer Z1 wide-field inverted microscope using an LD Pan neofluar 40x/0.6 objective. For the recording, illumination was reduced to 10% to minimize bleaching and images were taken every 500 ms for 5 min. Time-lapse movies were analyzed with FIJI; first aligned with the StackReg plugin, background was subtracted, the AVA cell body was manually selected and GFP intensities were quantified over the whole recoding time. Each spontaneous activation was defined on the profile and analyzed separately. The average of 10 time frames before the start of activation was used as baseline (F_0). For normalization, the mean of 10 frames after reaching maximal intensity was considered as 100% activity. For inactivation kinetics intensities were normalized and the mean of 10 frames prior the inactivation was used to define F_0 intensity and signal change was monitored until the intensity reached the baseline.

Yeast one-hybrid screen

The 114 bp *mps-2* promoter element was first inserted in front of the *HIS3* fused to *Kluyveromyces lactis URA3* gene. Amplified PCR product containing *URA3* locus specific flanking arms was transformed with the lithium-acetate method and integrated in the *URA3* locus of Y8930 yeast strain. The positive strains were confirmed with PCR, gel electrophoresis and sequencing. Library screening was performed by mating the bait strain with Y8800 yeast cells carrying a mixed stage *C. elegans* cDNA library fused to Gal4-AD (approx. $2x10^7$ clones) and interactions were selected on His- plates supplemented with 5mM 3-Amino-1,2,4-triazole (3-AT). Selected colonies were picked, and the isolated prey clones were identified by sequencing with Gal4AD and ADH1-terminator primers. The prey plasmids were isolated and transformed into the bait strain, and selected for His requirement in presence of different concentrations of 3-AT (1mM-20mM) to recapitulate the interaction.

Worm survival

For lifespan, synchronized L1 animals were put on NGM plates and grown at 20°C for 3 days. On three replicate NGM plates supplemented with 100 μg/ml FUDR 50 young adult worms were put, transferred once more 24 h later and were monitored daily for viability over the whole lifespan.

QUANTIFICATION AND STATISTICAL ANALYSIS

Samples were collected in a non-blinded way and effect sizes were not defined *a priori*. Data was analyzed and plotted using Prism 7. Data is represented as Tukey's boxplot unless indicated. Normality of the data was tested using D'Agostino & Pearson normality test. Main effects and interaction terms were tested with ANOVA and tests for significance were done with F-tests using sums-of-squares type I. For Ca^{2+} kinetic measurements a non-linear asymmetric sigmoidal regression using least-squares fit was used. Difference of datasets was tested using sum-of-squares F-test. Significance between datasets was tested using post hoc t tests and p value was adjusted for the number of tests performed in the analysis with either Dunnett or Bonferroni-correction ($p_{bonf} < 0.05$). For detailed statistics see Table S1.